Electronic Supplementary Material (ESI) for CrystEngComm.

Anion templated crystal engineering of halogen bonding tripodal tris(halopyridinium) compounds

Émer M. Foyle and Nicholas G. White*

Research School of Chemistry, The Australian National University, Canberra, ACT, Australia

Email: nicholas.white@anu.edu.au
URL: www.nwhitegroup.com

Characterisation

General remarks for characterisation.

NMR spectra were collected on Bruker Advance 400 or Bruker Advance 600 spectrometers and were referenced to the residual solvent peak.[1] Electrospray ionisation mass spectroscopy data were acquired on a Micromass Waters ZMD spectrometer.

NMR data

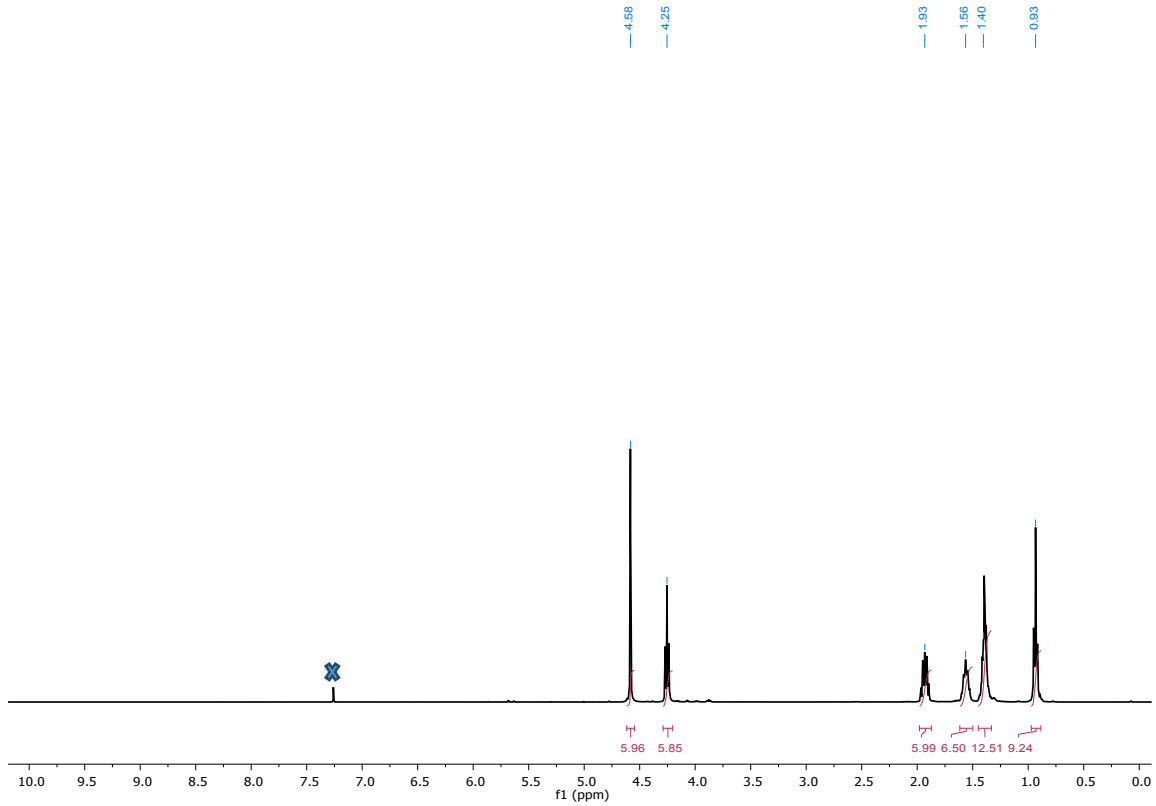

Figure S1: ^{1}H NMR spectrum of **9**. The cross denotes the peak that corresponds to incompletely deuterated solvent ($CDCl_3$, 400 MHz, 298 K).

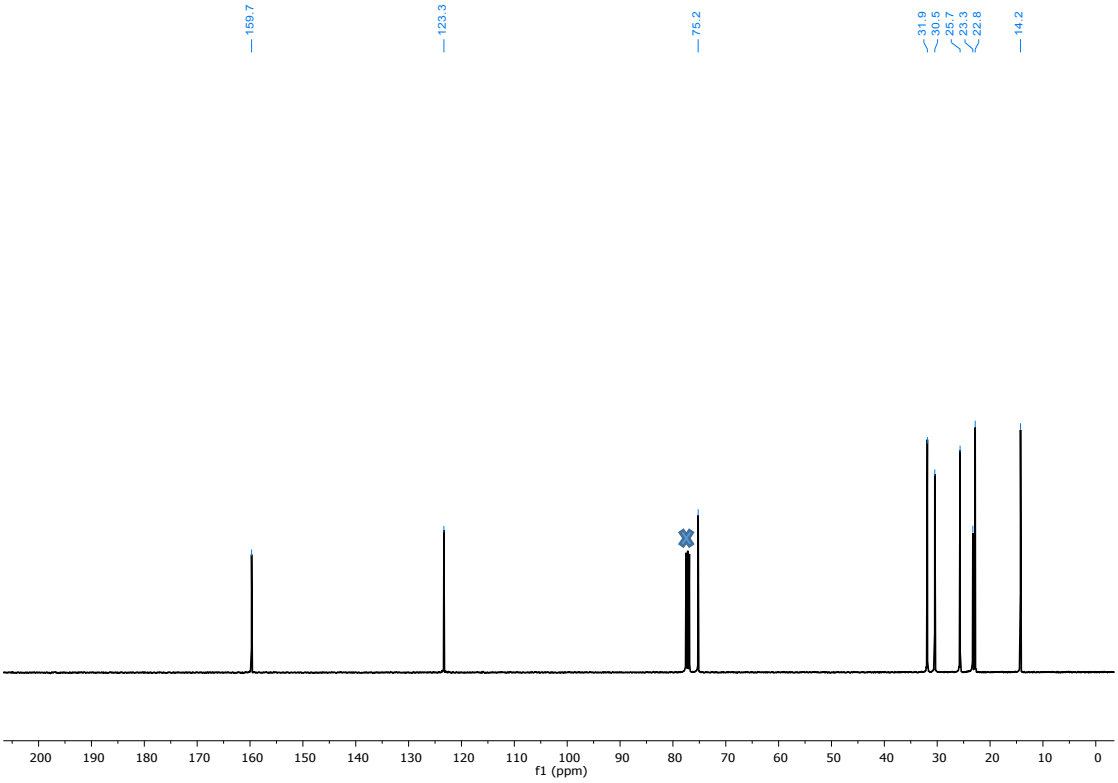

Figure S2: ^{13}C NMR spectrum of **9**. The cross denotes the peak that corresponds to the NMR solvent ($CDCl_3$, 101 MHz, 298 K).

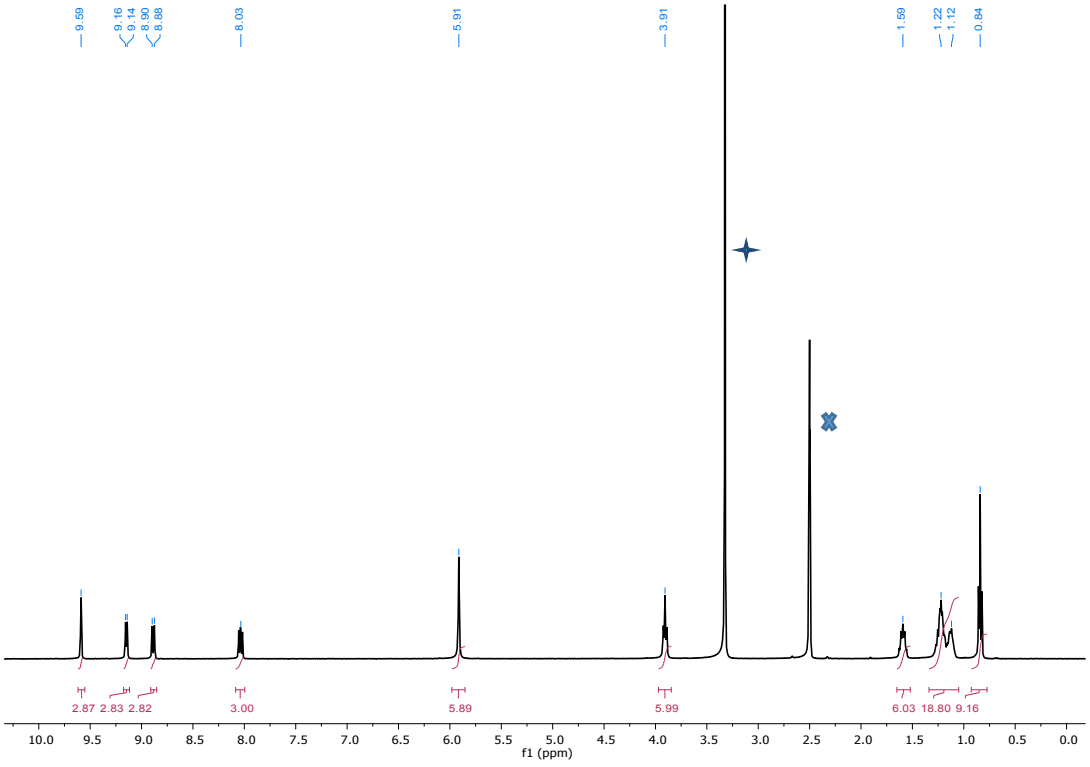

Figure S3: ^{1}H NMR spectrum of **3·Br$_3$**. The cross denotes the peak that corresponds to incompletely deuterated solvent and the star corresponds to the water peak (d^6-DMSO, 400 MHz, 298 K).

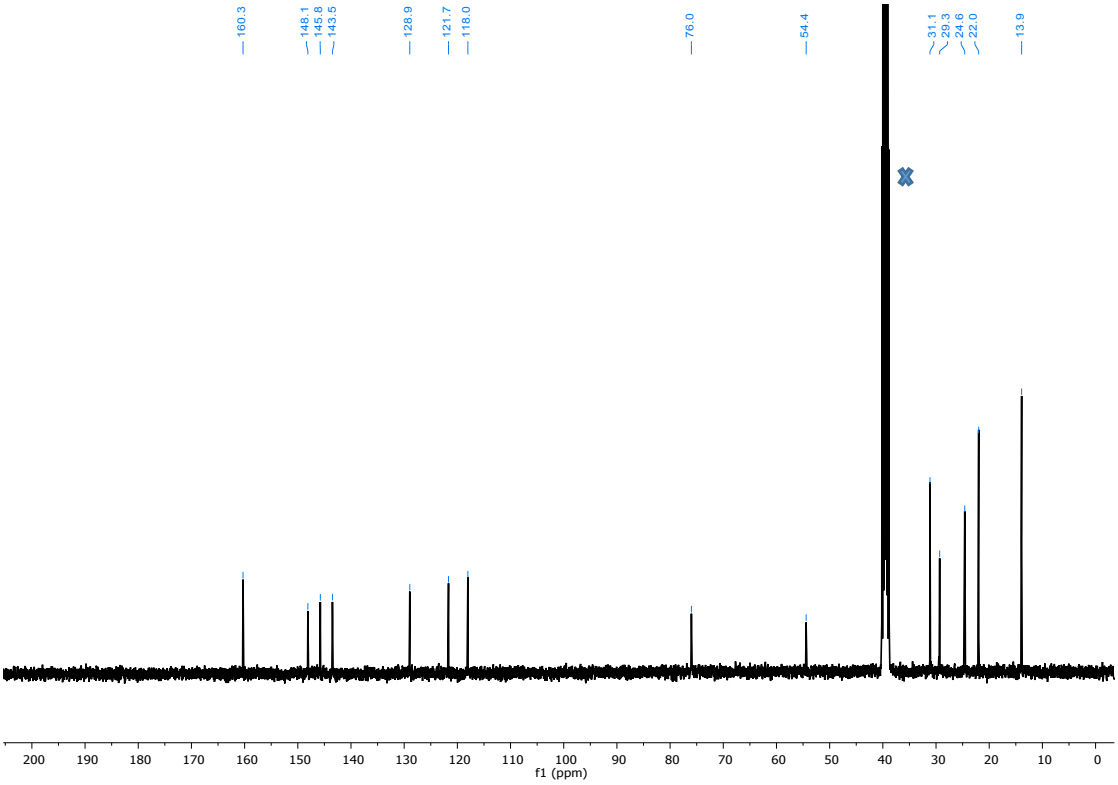

Figure S4: ^{13}C NMR spectrum of **3·Br$_3$.** The cross denotes the peak from the NMR solvent (*d*^{6}-DMSO, 101 MHz, 298 K).

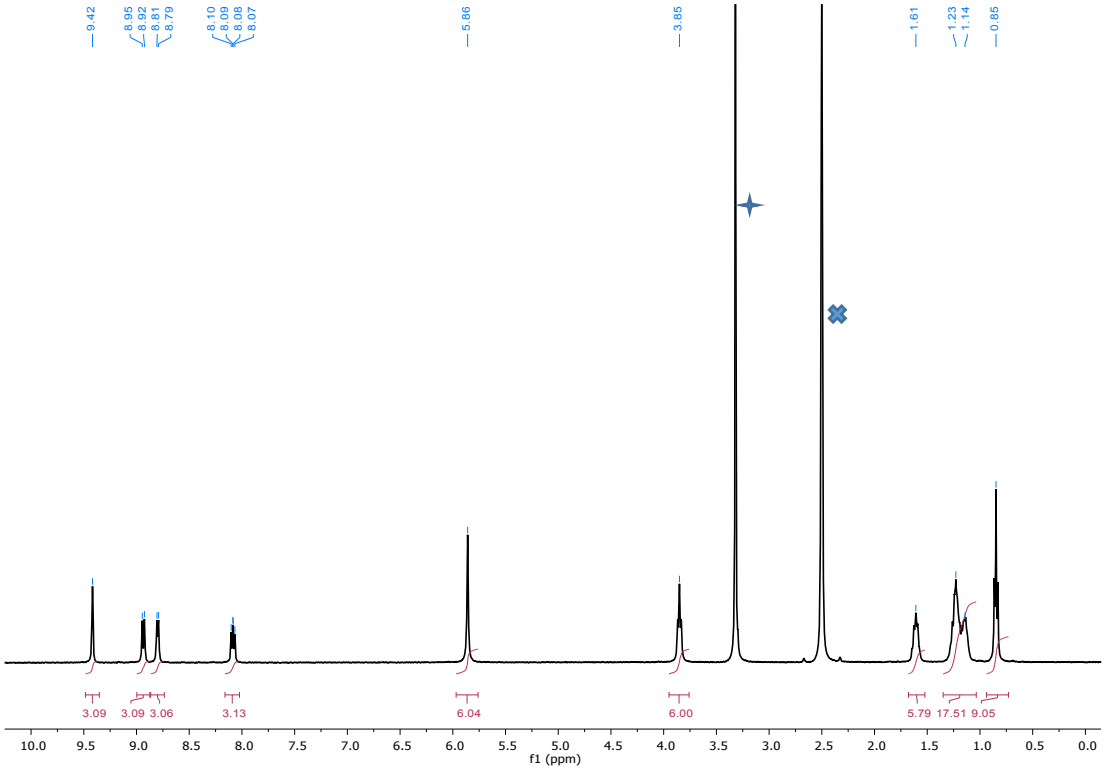

Figure S5: ^{1}H NMR spectrum of **3·(PF$_6$)$_3$**. The cross denotes the peak that corresponds to incompletely deuterated solvent and the star denotes the water peak (d^6-DMSO, 400 MHz, 298 K).

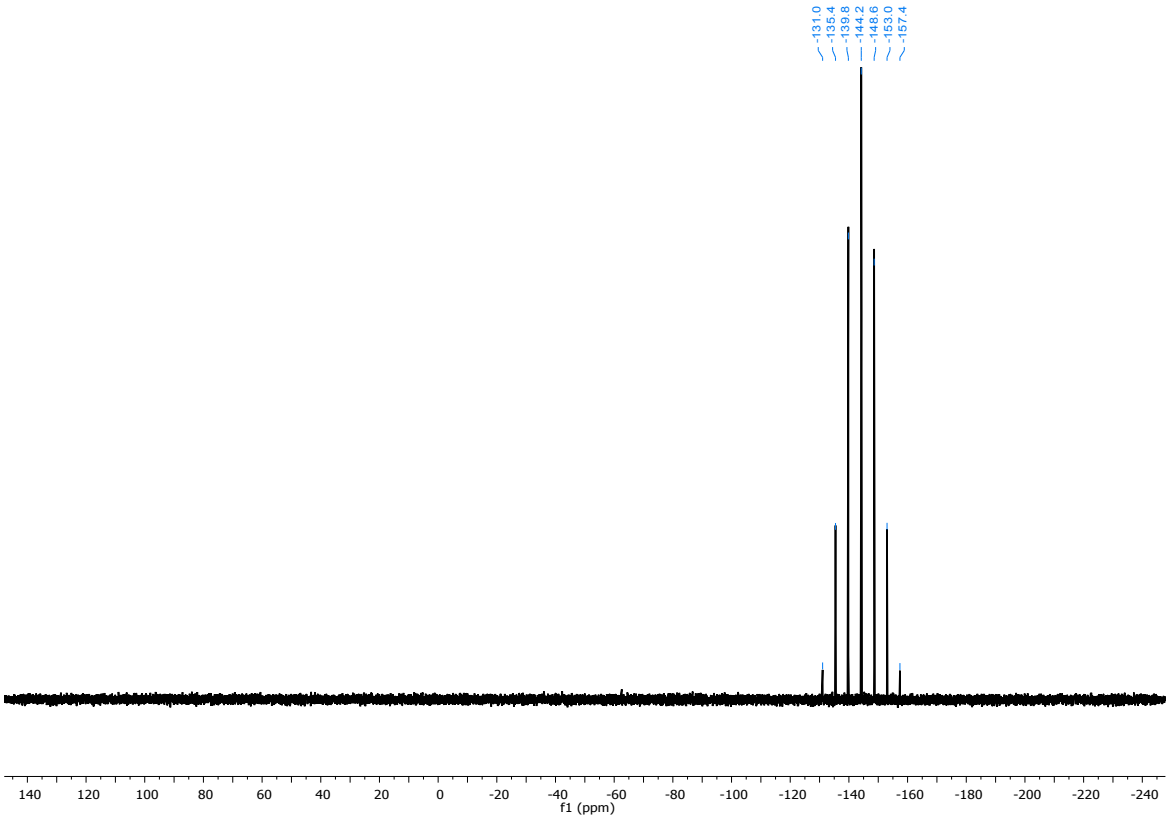

Figure S6: ^{31}P NMR spectrum of **3·(PF$_6$)$_3$** (*d*^{6}-DMSO, 161 MHz, 298 K).

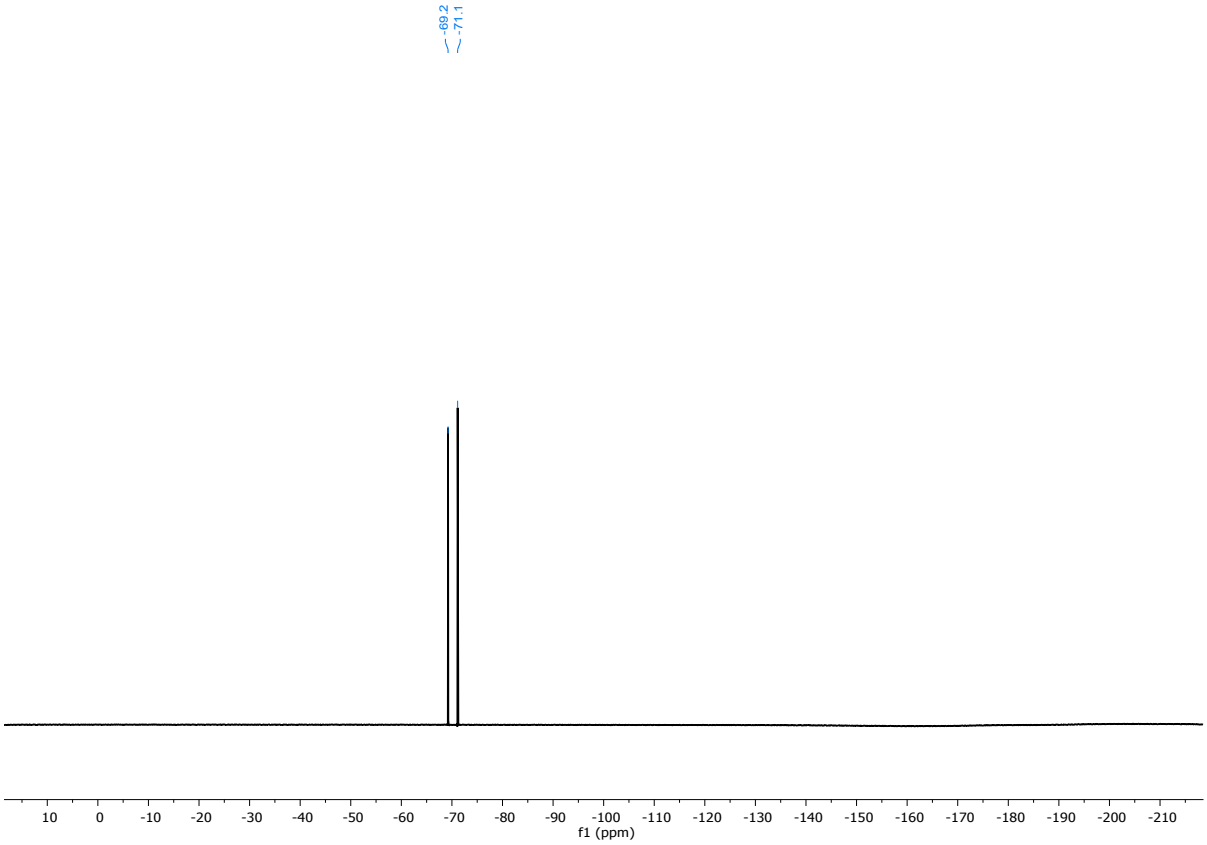

Figure S7: ^{19}F NMR spectrum of **(3·PF$_6$)$_3$** (*d*^{6}-DMSO, 376 MHz, 298 K).

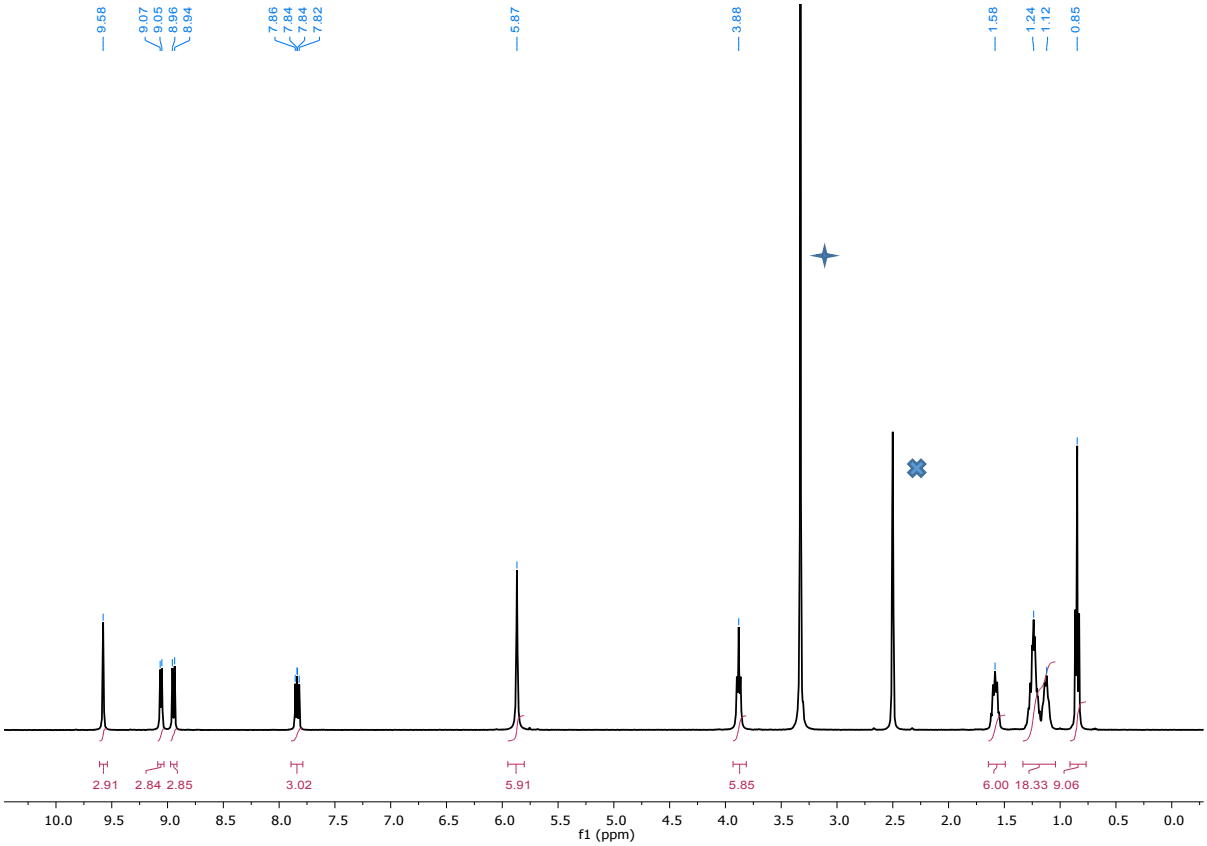

Figure S8: ^{1}H NMR spectrum of **4·Br$_3$.** The cross denotes the peak that corresponds to incompletely deuterated solvent and the star denotes the water peak (*d*^{6}-DMSO, 400 MHz, 298 K).

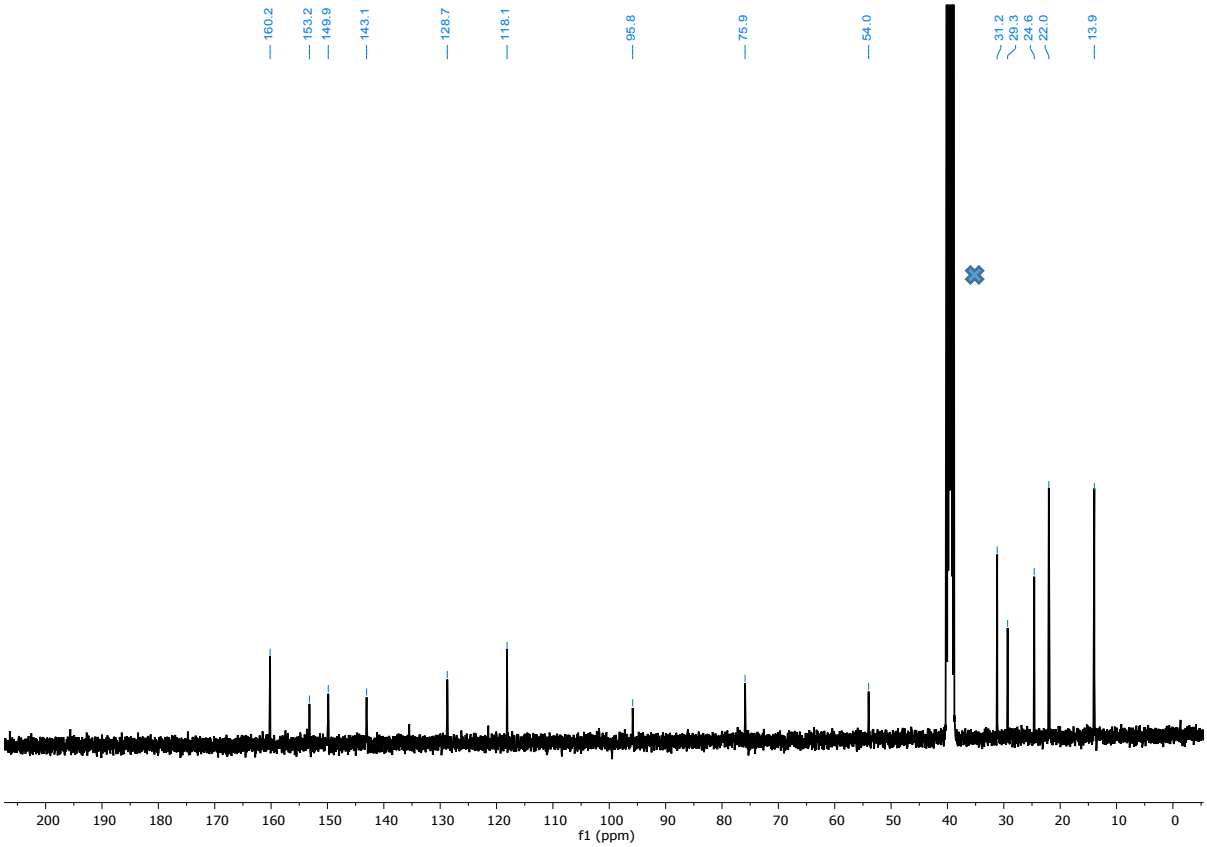

Figure S9: ^{13}C NMR spectrum of **4·Br$_3$.** The cross denotes the peak from the NMR solvent (*d*^{6}-DMSO, 101 MHz, 298 K).

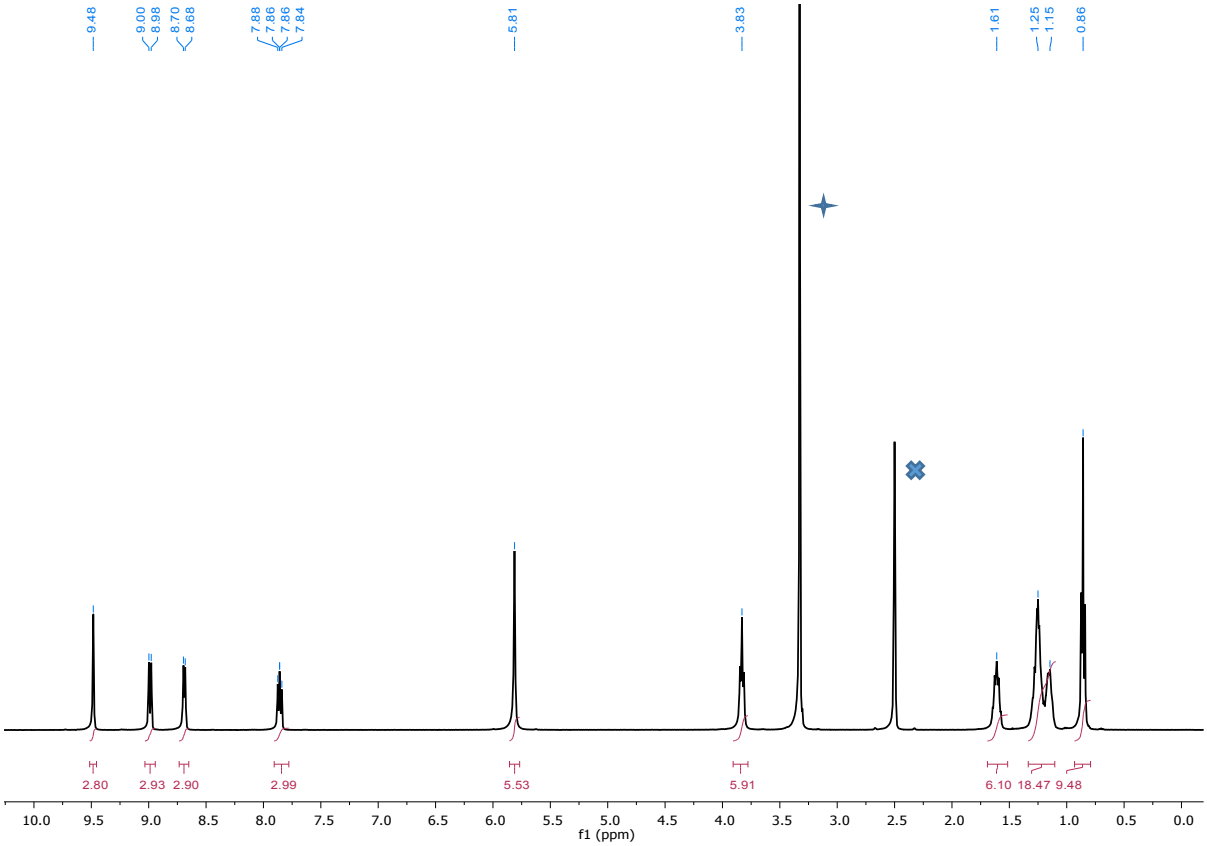

Figure S10: ^{1}H NMR spectrum of **4·(PF$_6$)$_3$**. The cross denotes the peak that corresponds to incompletely deuterated solvent and the star denotes the water peak (d^6-DMSO, 400 MHz, 298 K).

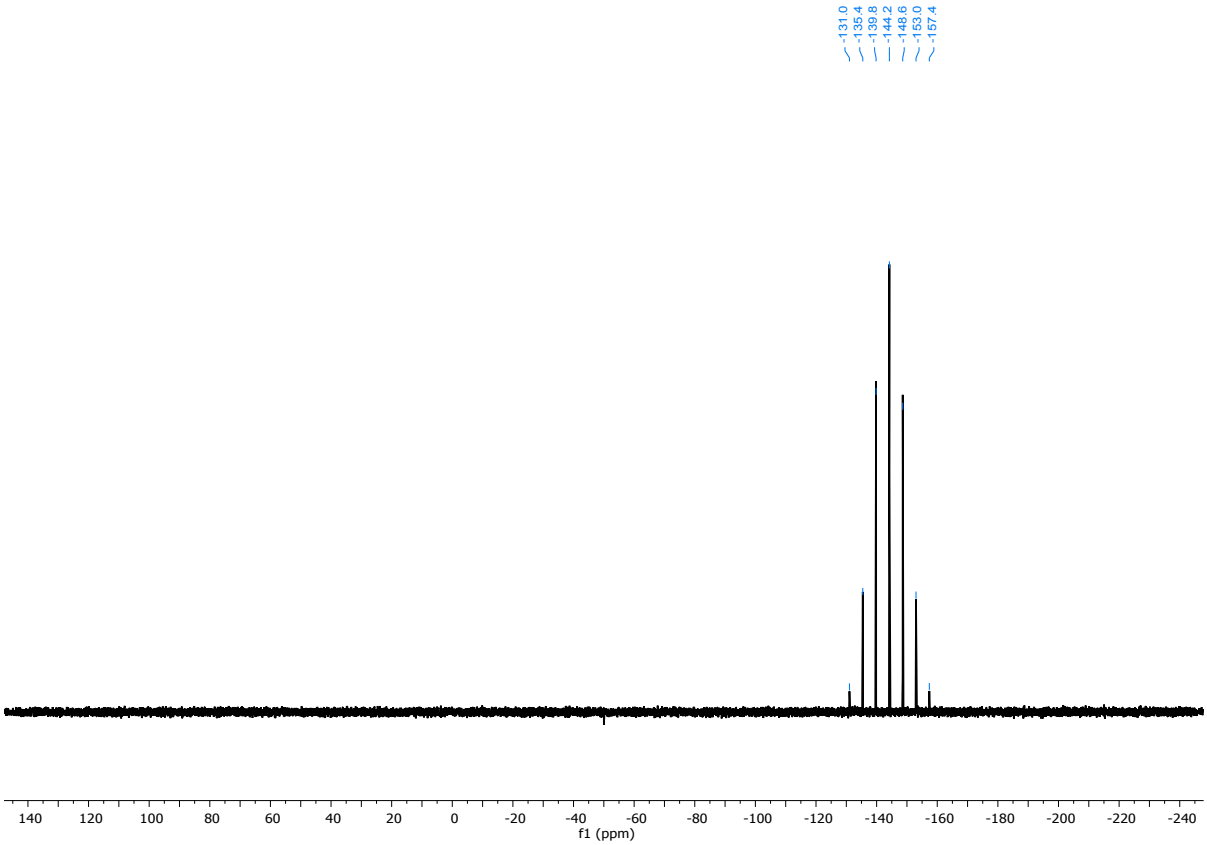

Figure S11: ^{31}P NMR spectrum of **4·(PF$_6$)$_3$** (d^6-DMSO, 161 MHz, 298 K).

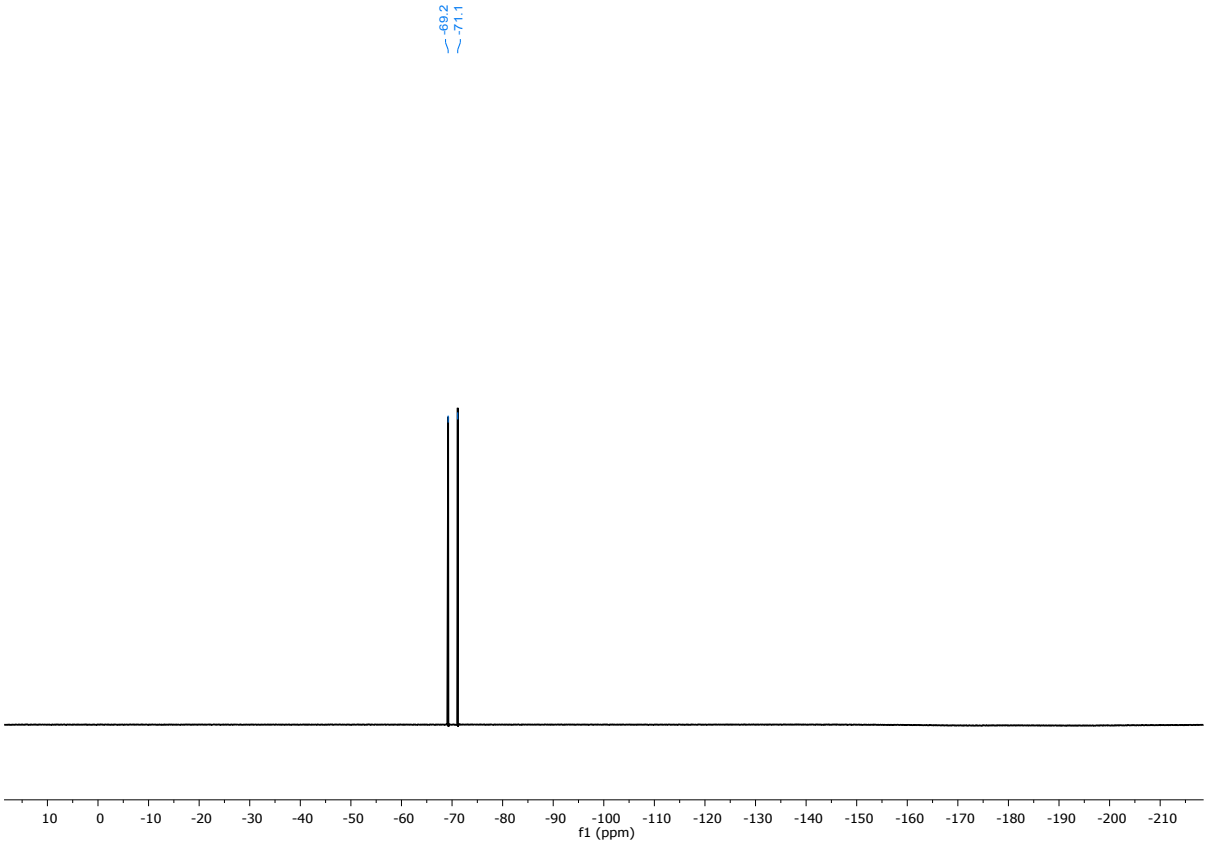

Figure S12: ^{19}F NMR spectrum of **4·(PF$_6$)$_3$** (*d*^{6}-DMSO, 376 MHz, 298 K).

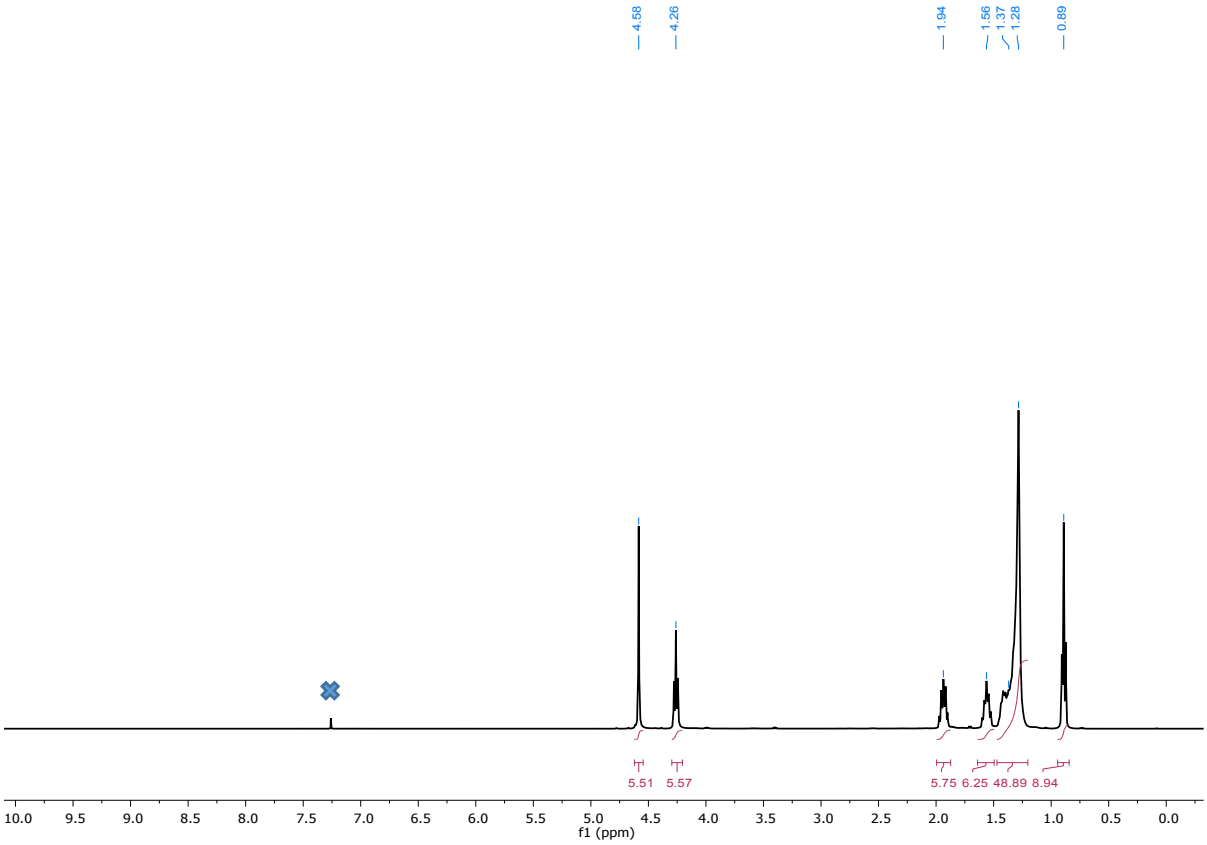

Figure S13: ^{1}H NMR spectrum of **10**. The cross denotes the peak that corresponds to incompletely deuterated solvent ($CDCl_3$, 400 MHz, 298 K).

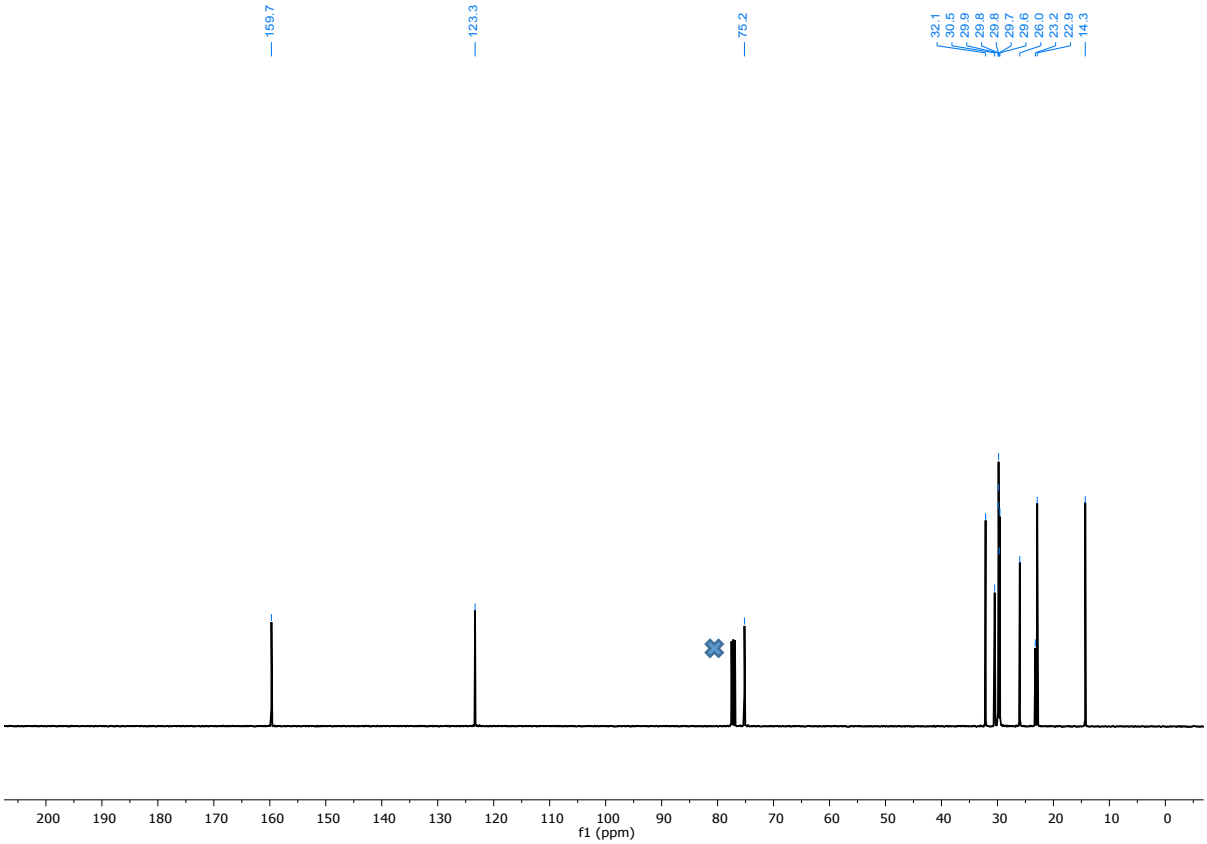

Figure S14: ^{13}C NMR spectrum of **10**. The cross denotes the peak from the NMR solvent ($CDCl_3$, 101 MHz, 298 K).

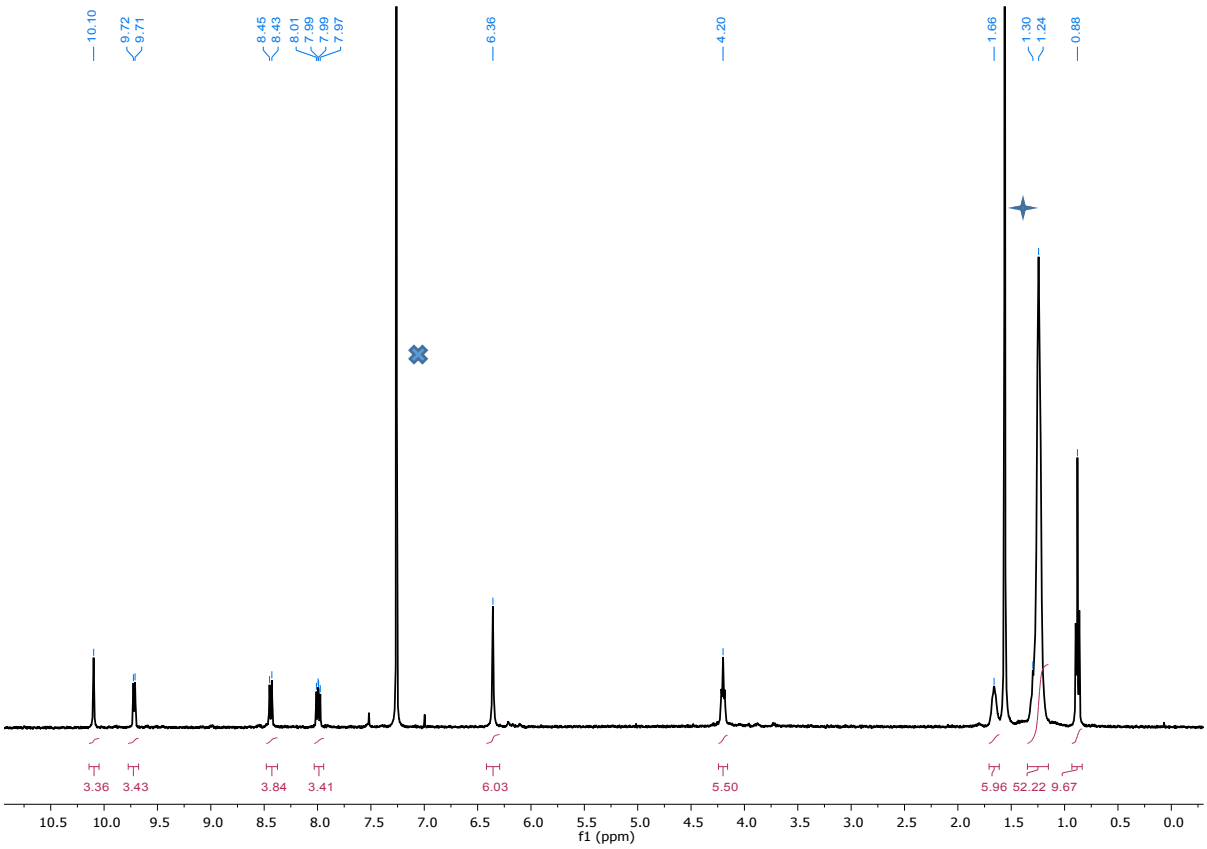

Figures S15: ^{1}H NMR spectrum of **5·Br$_3$**. The cross denotes the peak that corresponds to incompletely deuterated solvent and the star denotes the water peak ($CDCl_3$, 400 MHz, 298 K).

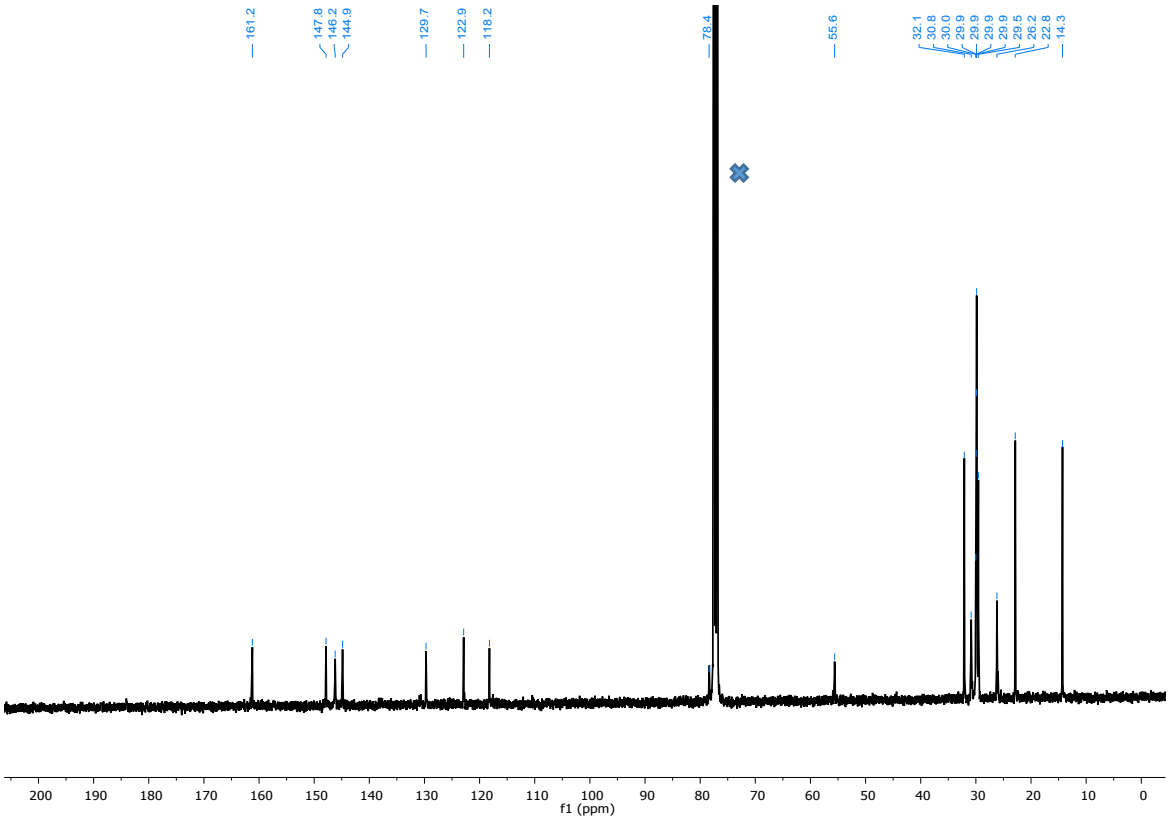

Figure S16: ^{13}C NMR spectrum of **5·Br$_3$**. The cross denotes the peak from the NMR solvent ($CDCl_3$, 101 MHz, 298 K).

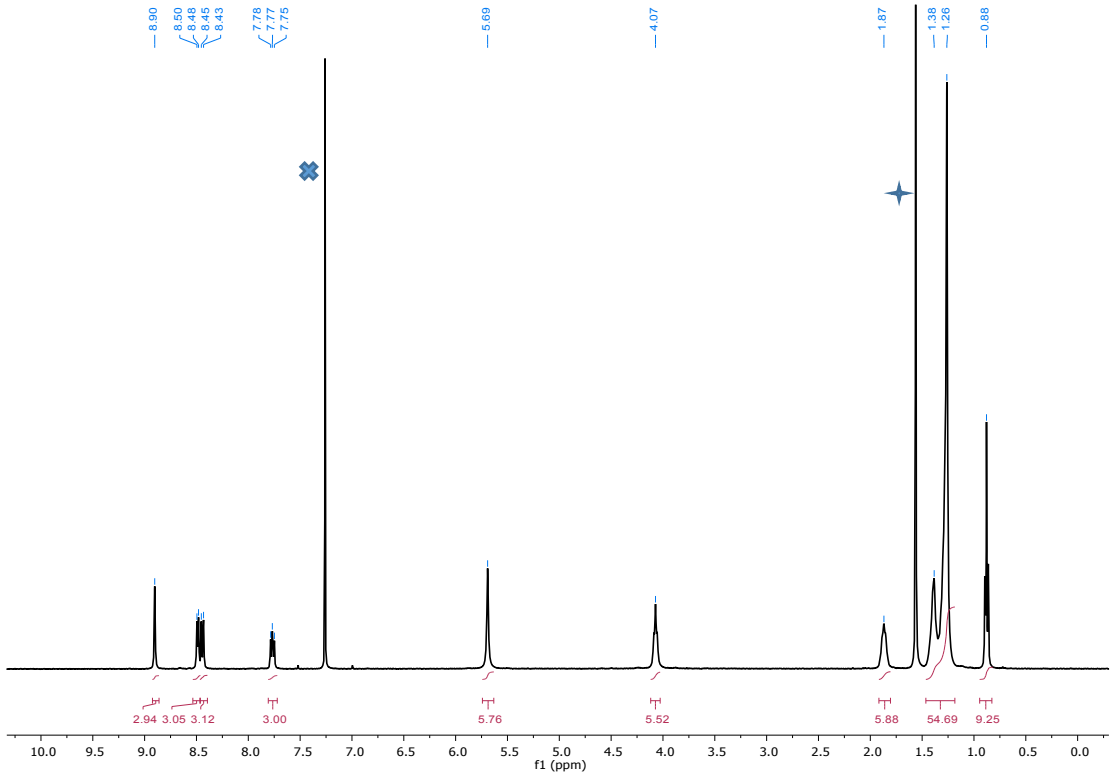

Figure S17: ^{1}H NMR spectrum of **5·(PF$_6$)$_3$**. The cross denotes the peak that corresponds to incompletely deuterated solvent and the star denotes the water peak ($CDCl_3$, 400 MHz, 298 K).

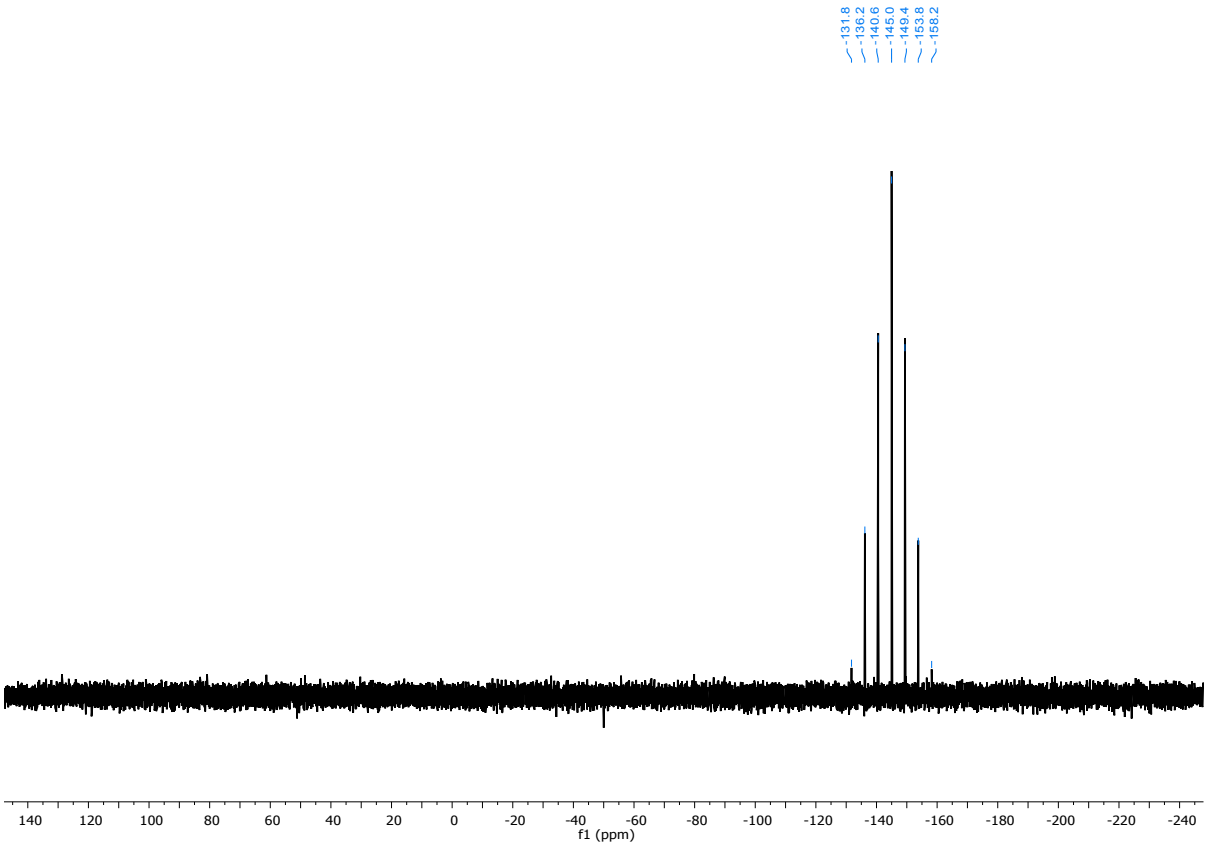

Figure S18: ^{31}P NMR spectrum of **5·(PF$_6$)$_3$** ($CDCl_3$, 161 MHz, 298K).

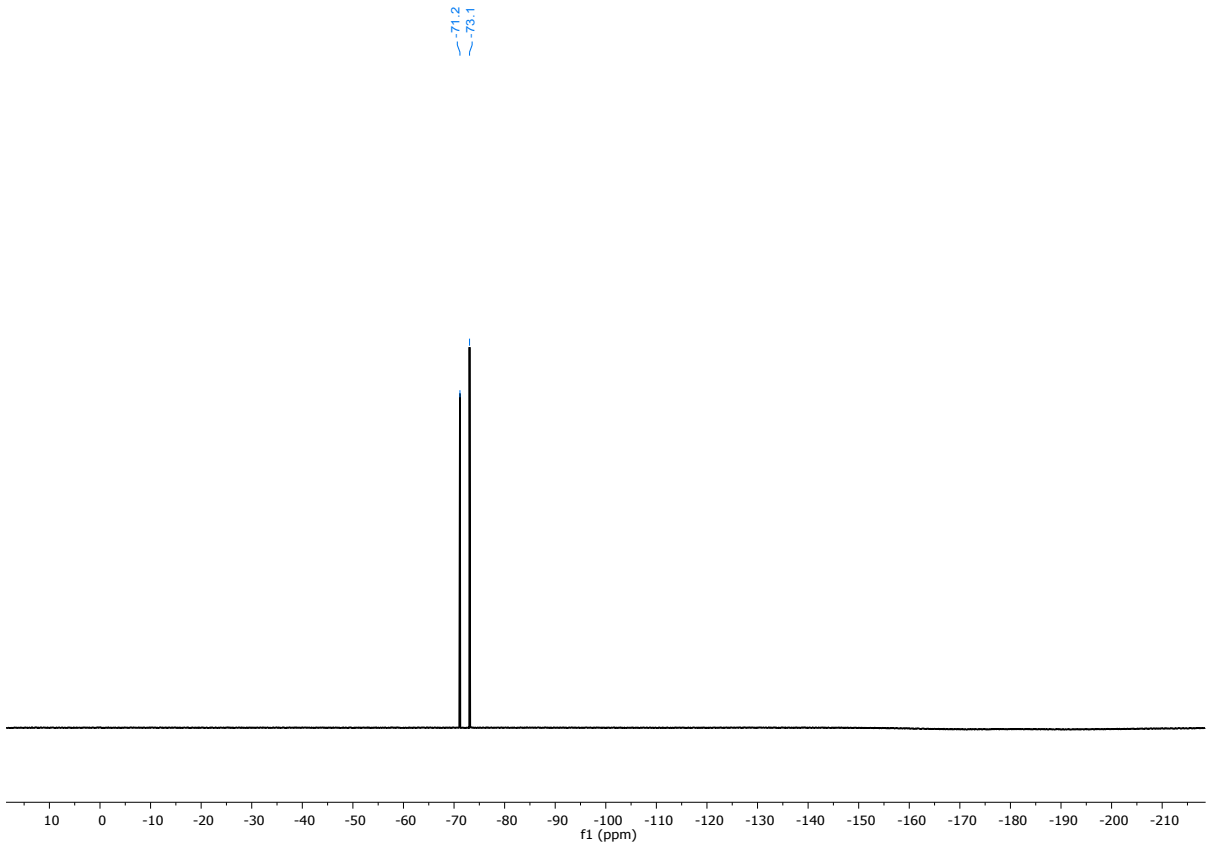

Figure S19: ^{19}F NMR spectrum of **5·(PF$_6$)$_3$** ($CDCl_3$, 376 MHz, 298 K).

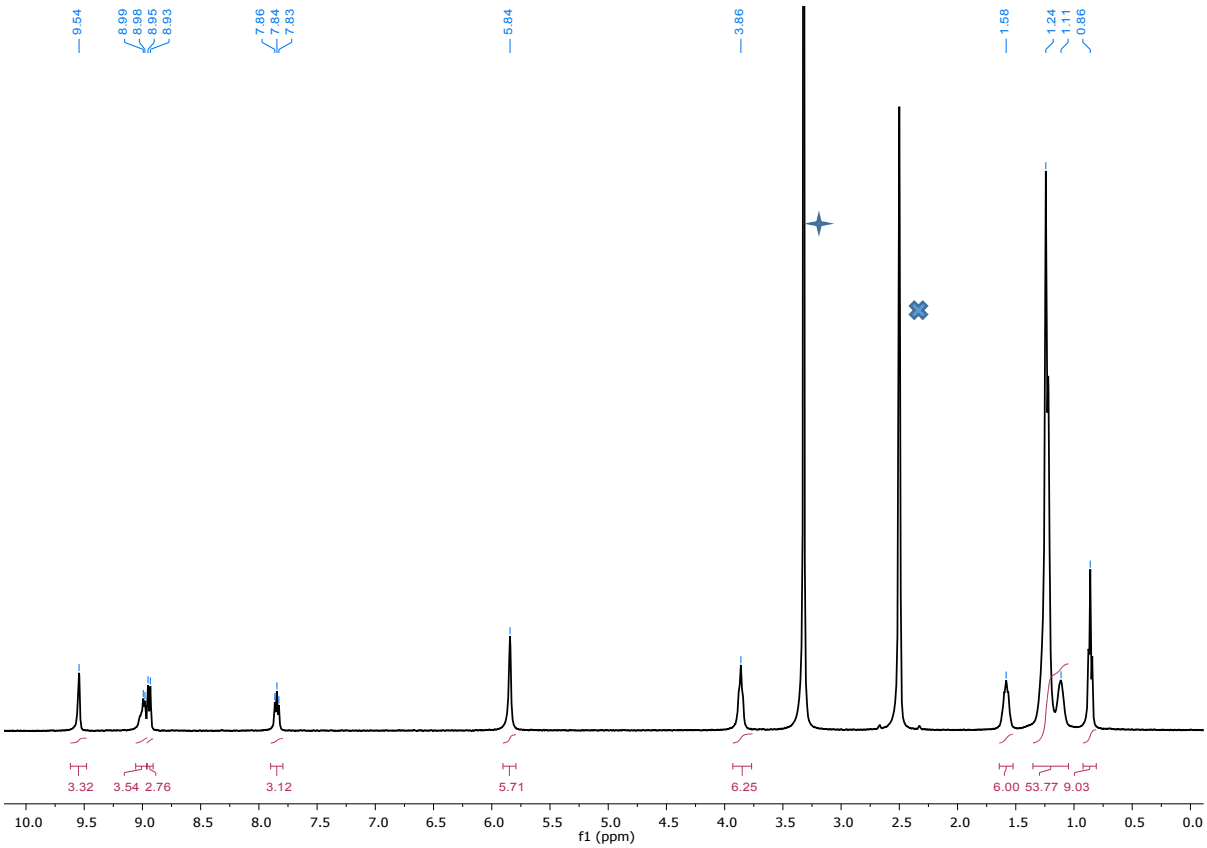

Figure S20: ^{1}H NMR spectrum of **6·Br$_3$.** The cross denotes the peak that corresponds to incompletely deuterated solvent and the star denotes the water peak (*d*^{6}-DMSO, 400 MHz, 298 K).

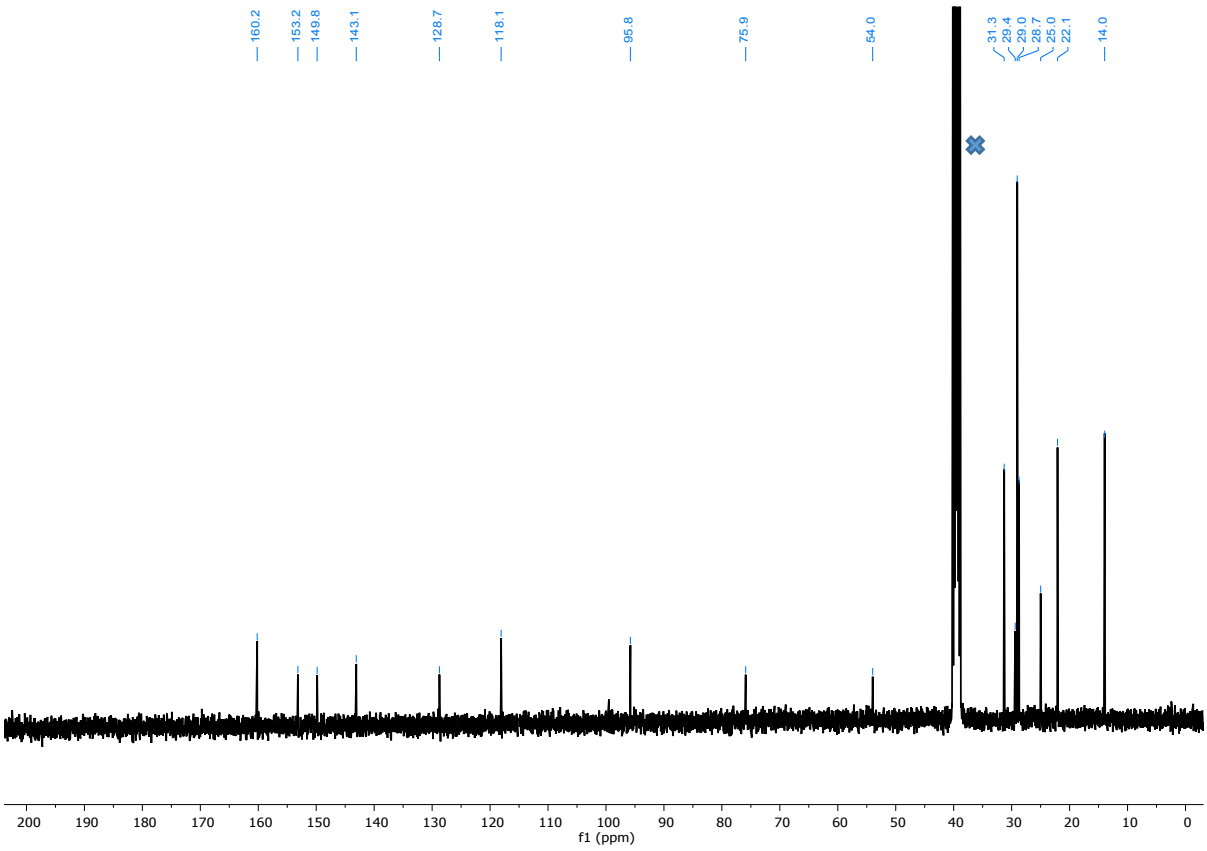

Figure S21: ^{13}C NMR spectrum of **6·Br$_3$**. The cross denotes the peak from the NMR solvent (*d*^{6}-DMSO, 101 MHz, 298 K).

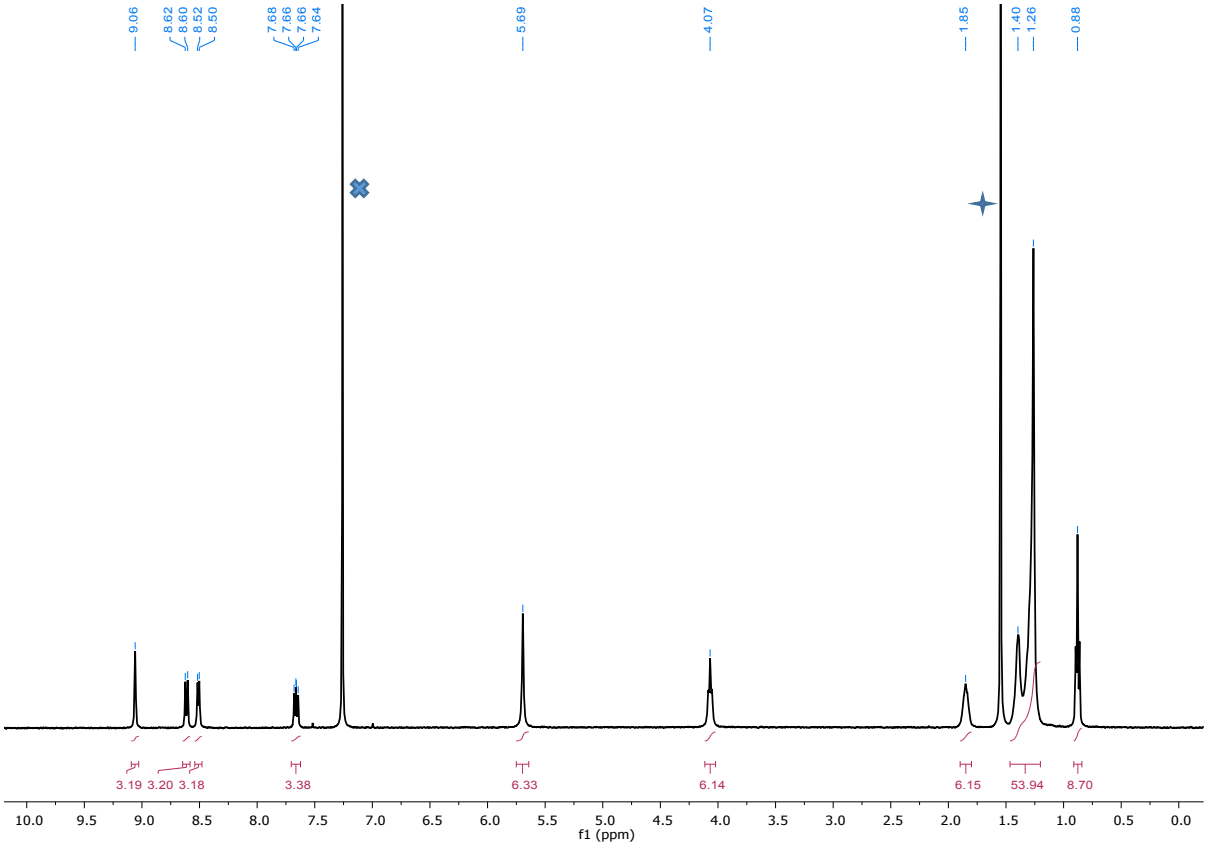

Figure S22: ^{1}H NMR spectrum of **6·(PF$_6$)$_3$**. The cross denotes the peak that corresponds to incompletely deuterated solvent and the star denotes the water peak ($CDCl_3$, 400 MHz, 298 K).

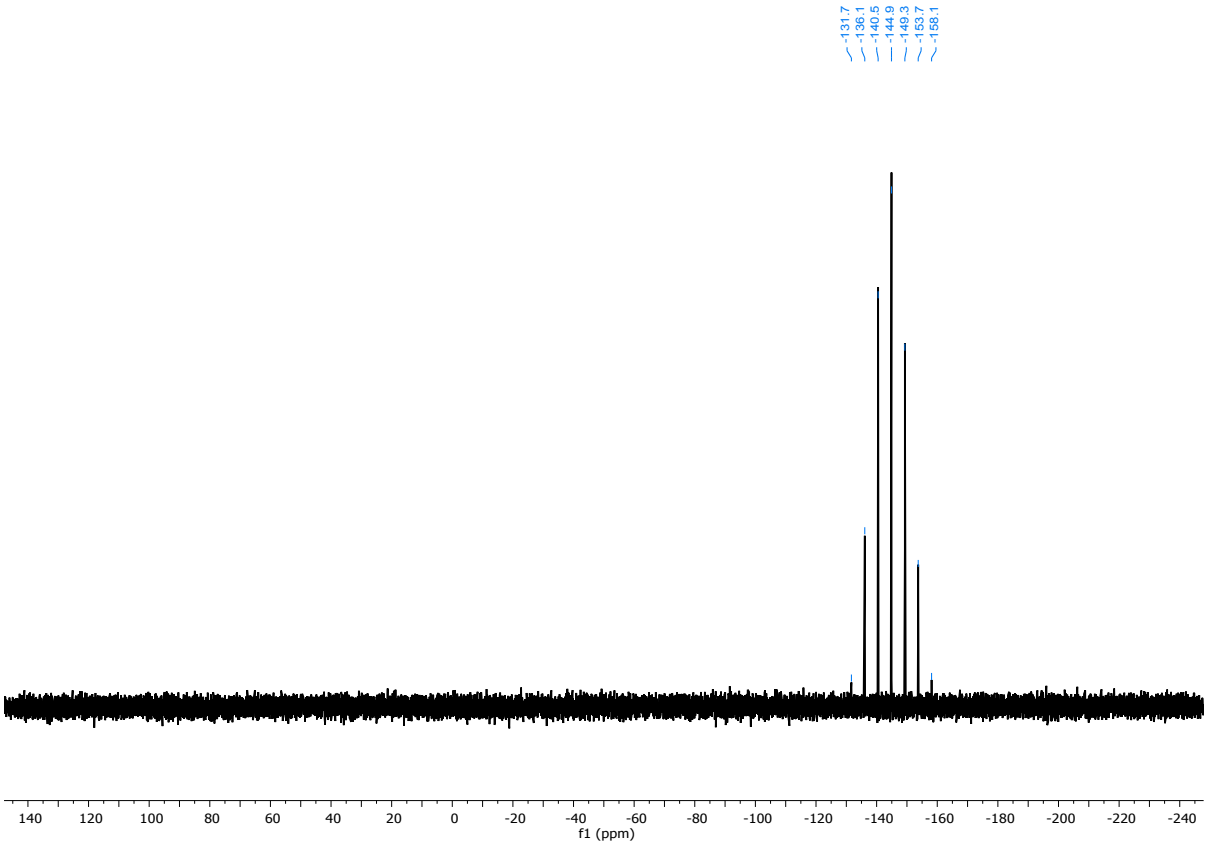

Figure S23: ^{31}P NMR spectrum of **6·(PF$_6$)$_3$** ($CDCl_3$, 161 MHz, 298 K).

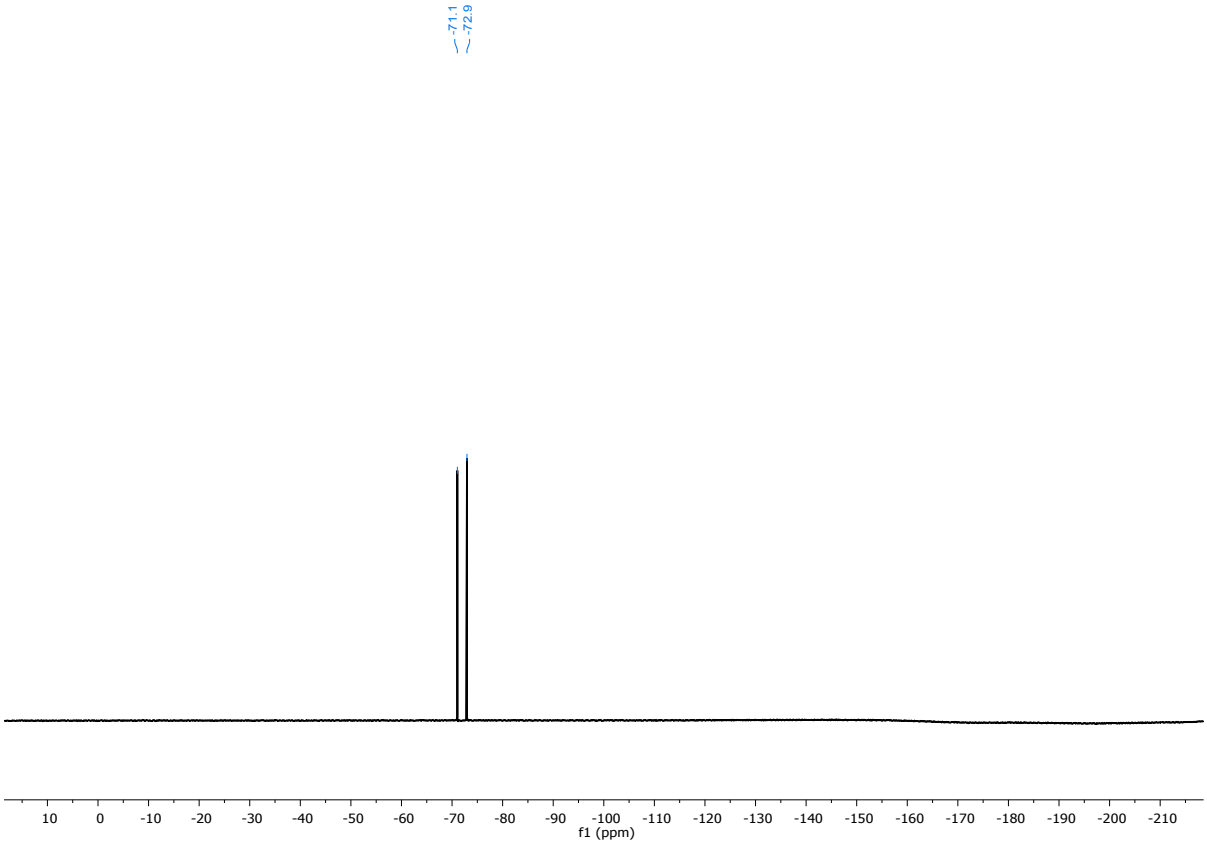

Figure S24: ^{19}F NMR spectrum of **6·$(PF_6)_3$** ($CDCl_3$, 376 MHz, 298 K).

Anion Binding Studies

Anion binding experiment protocol

The experiments were conducted at 298 K using a 600 MHz NMR instrument. The receptor concentration was initially 2.0 mmol L^{-1} with an initial volume of 0.50 mL. A 100 mM solution of an anion as its TBA salts was added. The increments of the anion addition were 0, 0.2, 0.4, 0.6, 0.8, 1.0, 1.2, 1.4, 1.6, 1.8, 2.0, 2.5, 3.0, 3.5, 4.0, 5.0, 7.0, 10.0. After the addition of the anion the NMR tube was inverted to fully mix the anion and receptor.

All binding constants were calculated using Bindfit.[2]

For all systems, the peak corresponding to H_4 (Figure S25) moved the most and so was used to calculate the binding constant.

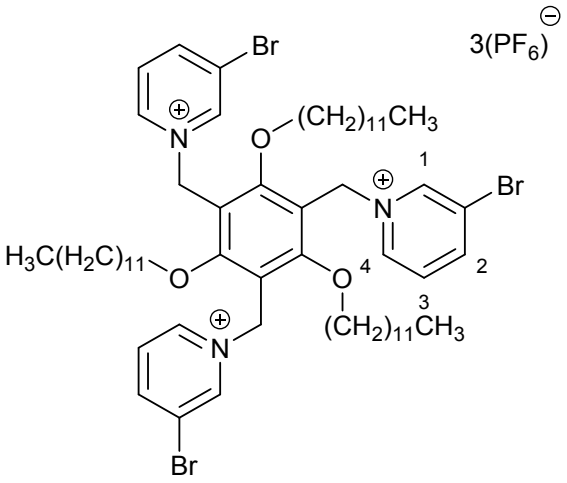

Figure S25: Structure of **5·(PF$_6$)$_3$** showing the numbering of H_1–H_4.

Anion binding data, spectra and fitted isotherms

5·(PF$_6$)$_3$ with TBA·Cl

The association constant was found to be 2608 (± 231) M^{-1}

Bindfit link: http://app.supramolecular.org/bindfit/view/b028168d-631c-4024-bad6-af1160727cd3

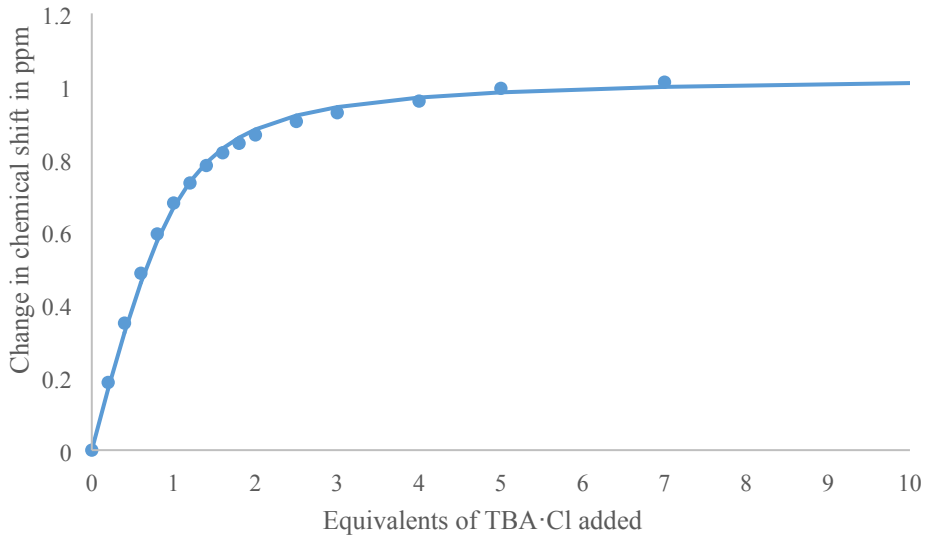

Figure S26: Movement of H_4 on the addition of TBA·Cl. Dots represent observed data points and line represent 1:1 binding isotherm fitted by Bindfit.[2]

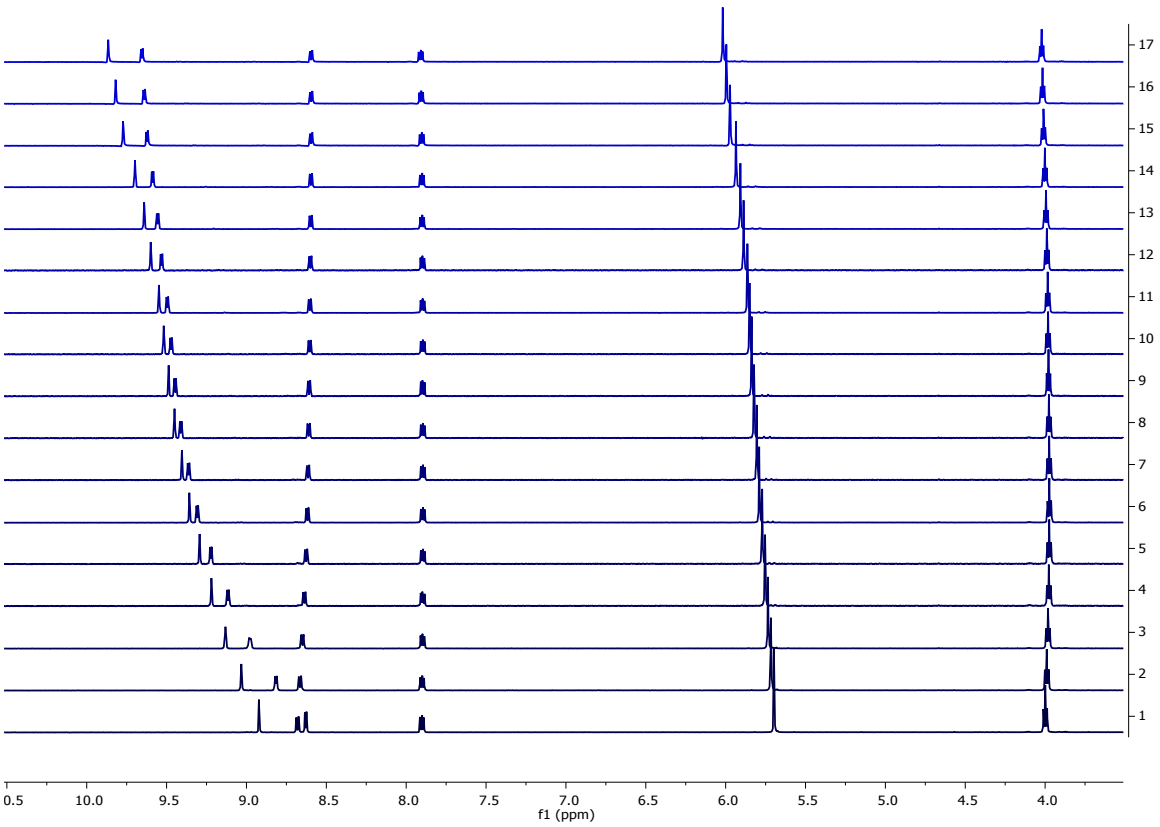

Figure S27: Truncated ^{1}H NMR spectra of **5·(PF$_6$)$_3$** on the addition of TBA·Cl (from 0 to 10 equivalents).

5·(PF$_6$)$_3$ with TBA·Br

The association constant was found to be 850(± 41) M^{-1}.
Bindfit link: http://app.supramolecular.org/bindfit/view/443a7a88-8fa7-4542-a00e-6422c41245e6

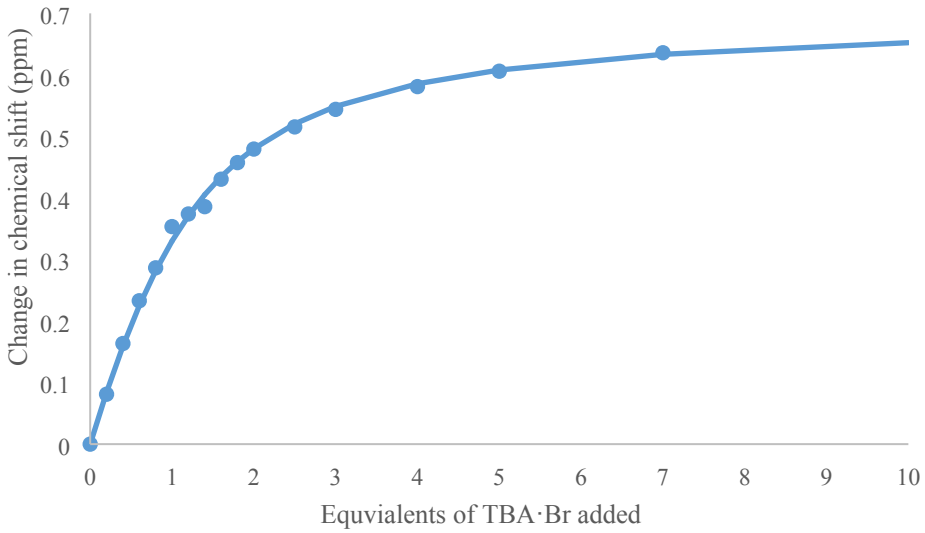

Figure S28: Movement of H_4 on the addition of TBA·Br. Dots represent observed data points and line represent 1:1 binding isotherm fitted by Bindfit.[2]

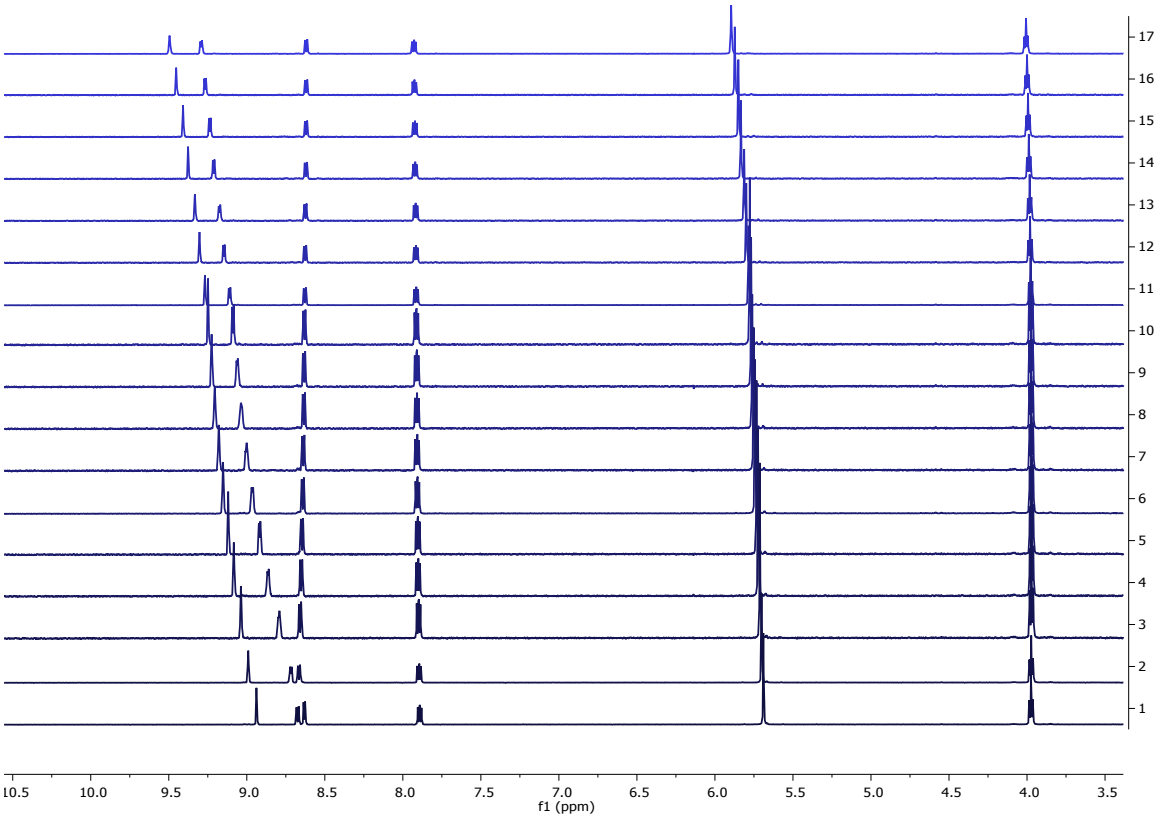

Figure S29: Truncated ^{1}H NMR spectra of **5·(PF$_6$)$_3$** on the addition of TBA·Br (from 0 to 10 equivalents).

5·(PF$_6$)$_3$ with TBA·I

The association constant value was found to be 544 ±(42) M^{-1}.
Bindfit link: http://app.supramolecular.org/bindfit/view/d3f02826-f146-4acc-a79c-f28fc3d47f61

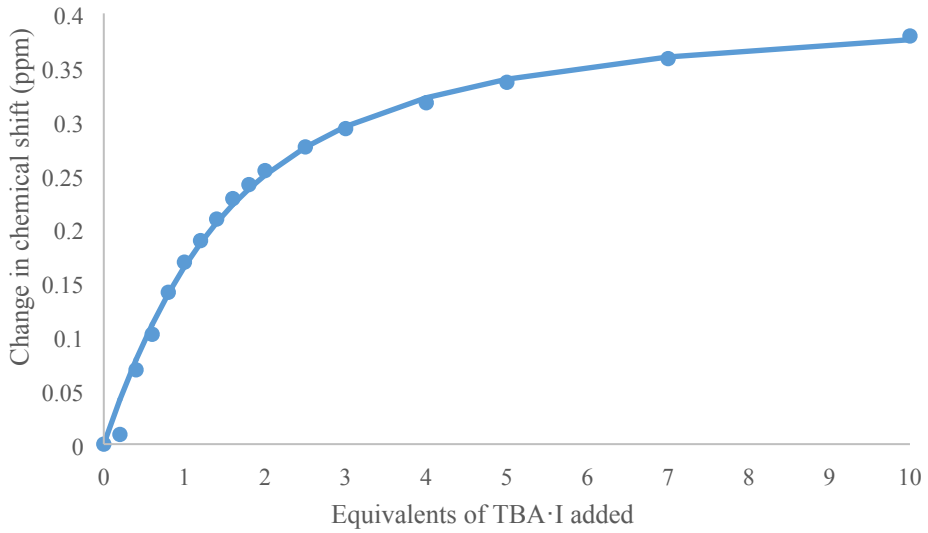

Figure S30: Movement of H_4 when 0-10 equivalents of TBA·I is added. Dots represent observed data points and the line represents 1:1 binding isotherm fitted by Bindfit.[2]

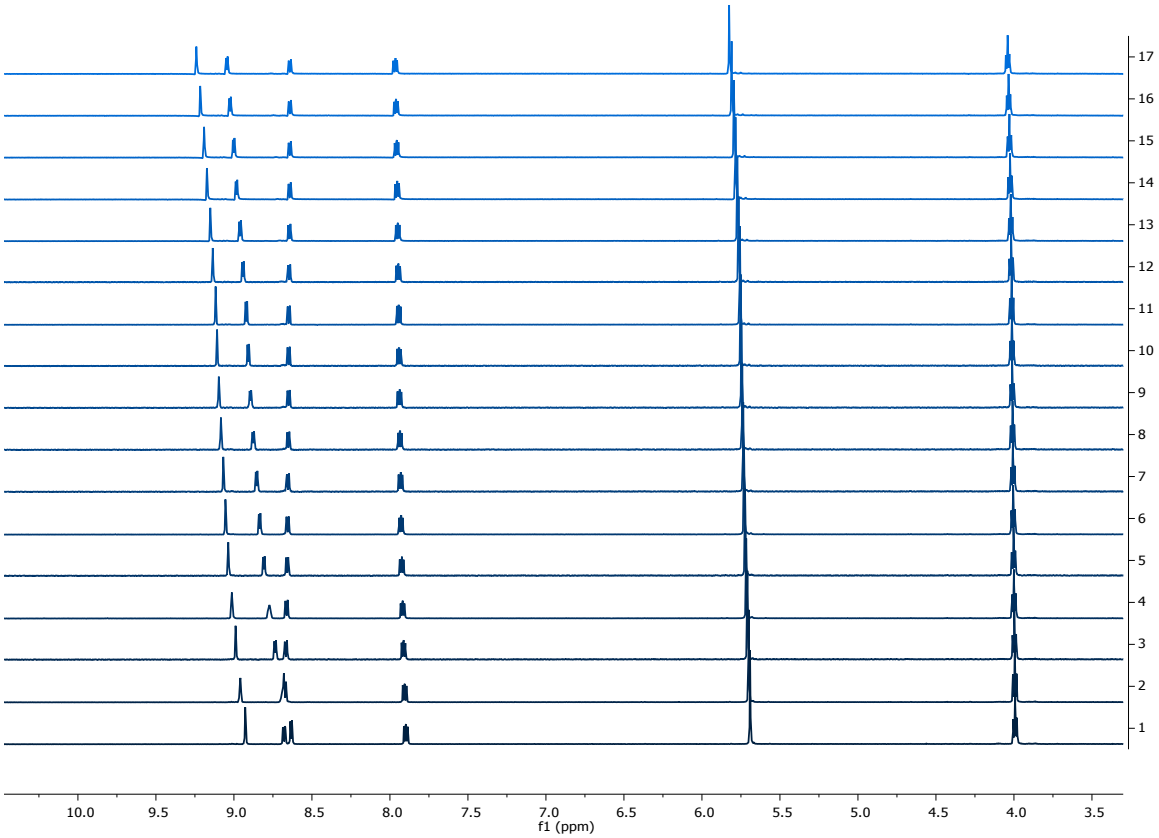

Figure S31: Truncated ^{1}H NMR spectra of **5·(PF$_6$)$_3$** with addition of TBA·I (from 0 to 10 equivalents).

5·(PF$_6$)$_3$ with TBA·OAc

The association constant was found to be 419(± 17) M^{-1}.
Bindfit link: http://app.supramolecular.org/bindfit/view/560d6ded-d01f-4e82-8d22-e477180b0765

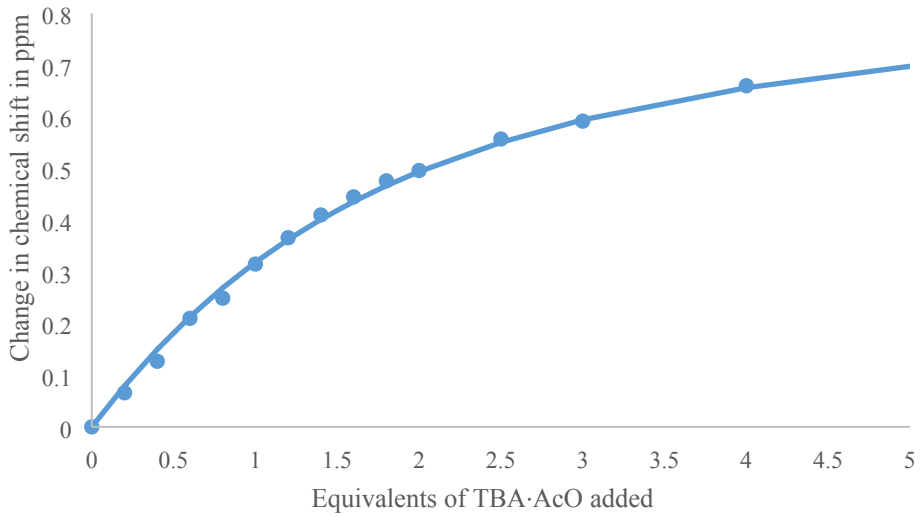

Figure S32: Movement of H_4 when 0-5 equivalents of TBA·OAc is added. Dots represent observed data points and the line represents 1:1 binding isotherm fitted by Bindfit.[2] Precipitate was observed after 5 equivalents were added.

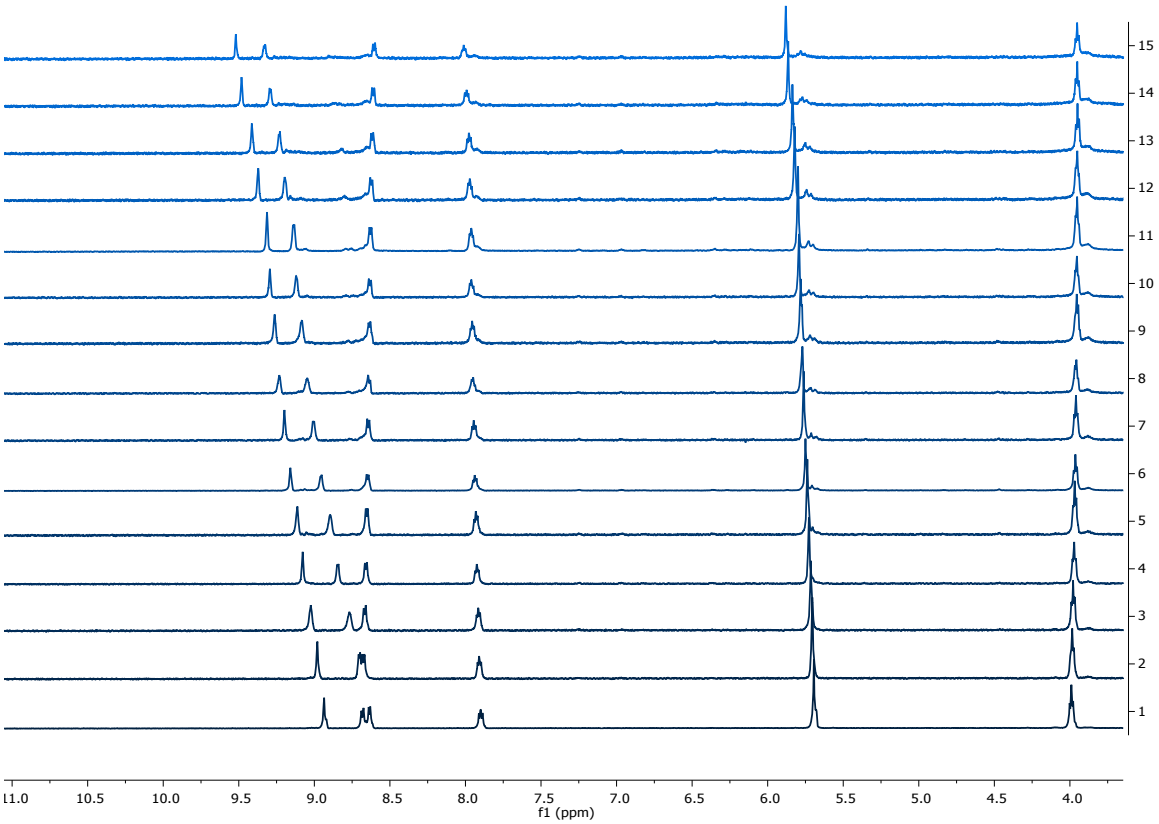

Figure S33: Truncated ^{1}H NMR spectra of **5·3(PF$_6$)$_3$** with addition of TBA·OAc (from 0 to 5 equivalents).

6·(PF$_6$)$_3$ with TBA·Cl

The association constant was found to be 2316(± 87) M^{-1}.
Bindfit link: http://app.supramolecular.org/bindfit/view/f652d63f-ac21-4eac-9a86-4abc669ca46a

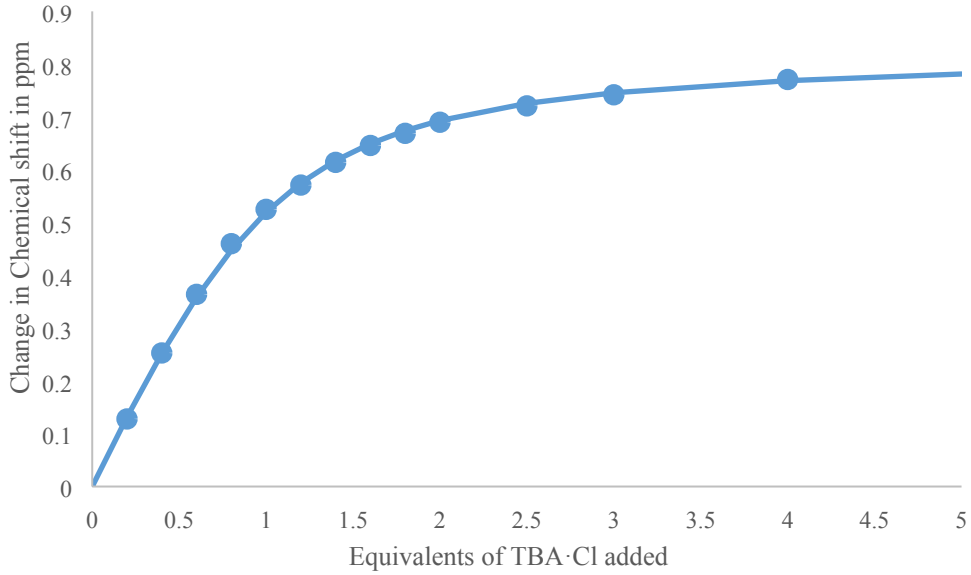

Figure S34: Movement of H_4 on **6·(PF$_3$)$_6$** when 0-5 equivalents of TBA·Cl is added. Dots represent observed data points and the line represents 1:1 binding isotherm fitted by Bindfit.[2] Precipitate observed after 5 equivalents were added.

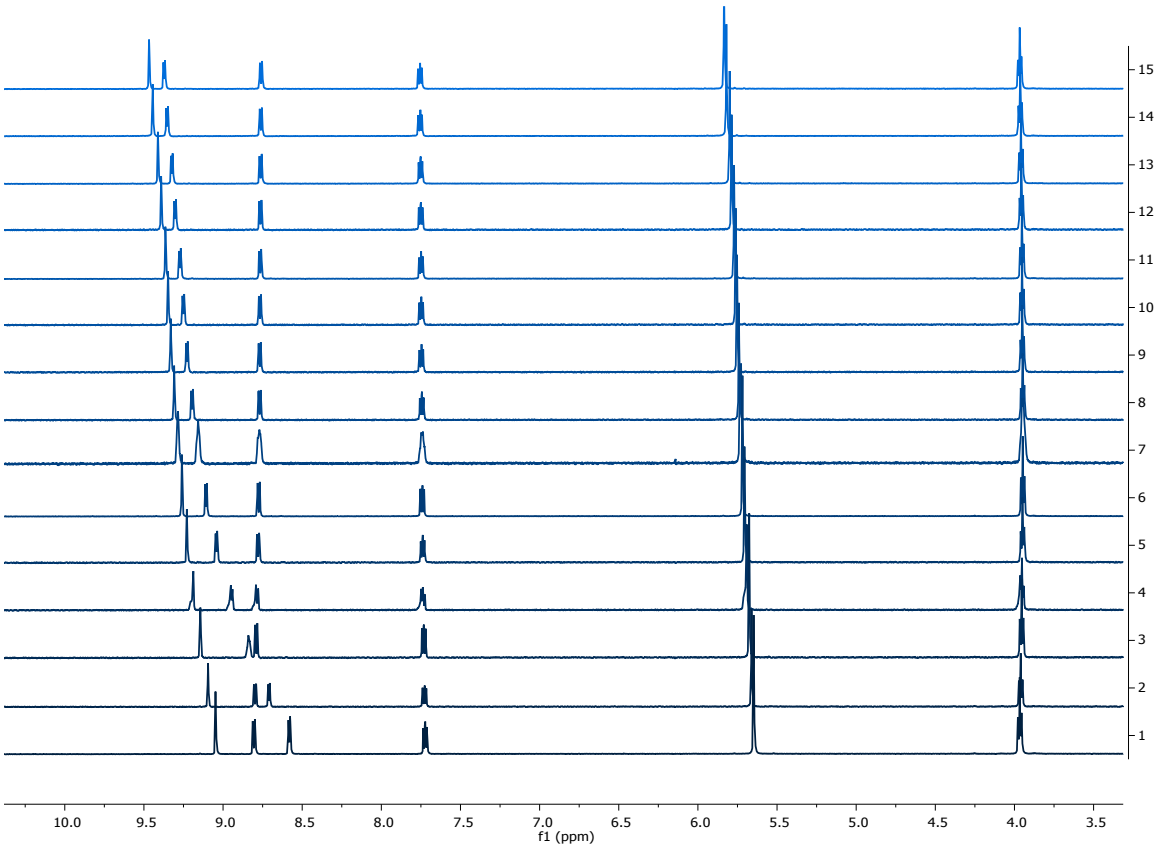

Figure S35: Truncated ^{1}H NMR spectra of **6·(PF$_6$)$_3$** with addition of TBA·Cl (from 0 to 5 equivalents).

X-ray Crystallography

General remarks for crystallography

Data for **3·$(PF_6)_3$**, **4·Cl·$(PF_6)_2$**, **4·I_3** and **3·Br_3** were collected on an Agilent SuperNova diffractometer using mirror-monochromated Cu Kα radiation. Crystals were cooled to 150 K using a Cryostream N_2 open-flow cooling device.[3] Raw frame data were processed using CrysAlisPro.[4]

The Data for **3·I_3**, **4·Br_3**, **3·Cl_3** and **4·$(PF_6)_{1.5}Br_{1.5}$**were collected at the Australian Synchrotron on the MX1 beamline using silicon double crystal monochromated synchrotron radiation at 100K.[5, 6] Raw frame data were collected using Blulce,[6] and data reduction, interframe scaling, unit cell refinement and absorption corrections were processed using XDS.[7]

The structures of **3·$(PF_6)_3$**, **3·Br_3** and **4·Cl·$(PF_6)_2$** were solved with ShelXT[8] and refined with ShelXL[9] using OLEX2.[10] All non-hydrogen atoms were refined with anisotropic displacement parameters. Hydrogen atoms were placed geometrically and with the same restraints as their parent atom.

The structures of **3·I_3**, **4·Br_3**, and **$4Br_{1.5}(PF_6)_{1.5}$** were solved with ShelXT[8] and refined with olex2.refine[11] using Gauss-Newton minimisation in OLEX2.[10]

Structures **4·I_3** and **3·Cl_3** were solved using SUPERFLIP[12] and refined within the *CRYSTALS* suite.[13,14]

Disorder in structure of 3·$(PF_6)_3$

In the structure of 3·$(PF_6)_3$ one of the bromine atoms is disordered over two possible positions, with occupancies of 84 and 16%. One of the PF_6^- anions is also disordered with occupancies of 64 and 36% for the two different sets of positions of the fluorine atoms.

Structure of 3·Cl_3

The crystals of **3·Cl_3** were weakly diffracting and even with synchrotron radiation the data obtained were weak and of poor quality although the overall conductivity of the structure was able to be determined unambiguously. Due to the quality of the data, it was necessary to use crystallographic restraints for most of the bond lengths and angles, as well as the thermal and vibrational ellipsoids to get a chemically sensible structure. One of the bromopyridinium rings is rotationally disordered over two positions with occupancies of 65 and 35% for these two positions.

Structure of PF_6^-/I^- salt of 4^{3+}

Diffusion of diethyl ether into a methanol solution of **4·$(PF_6)_3$** and 1.5 equivalents of TBA·I gave very low quality crystals of a mixed I/PF_6 salt of **4^{3+}**. Even with the use of synchrotron radiation, it was not possible to obtain satisfactory data for this structure and so a satisfactory refinement could not be achieved.

The unit cell parameters of this structure are very similar to those of **4·$Br_{1.5}$·$(PF_6)_{1.5}$** and the gross molecular structure of the PF_6^-/I^- structure seems to be that of a halogen bonded dimer [as is the case with **4·$Br_{1.5}$·$(PF_6)_{1.5}$**], however it does not appear that the structures are isostructural – for example, the PF_6^-/I^- contains a disordered anion site (where both PF_6^- and I^- are present on the same position). The partial occupancy iodide anion on this site does not appear to form a halogen bond to an iodopyridinium group (Figure S36), while in the structure of **4·$Br_{1.5}$·$(PF_6)_{1.5}$** all bromide anions take part in halogen bonding interactions.

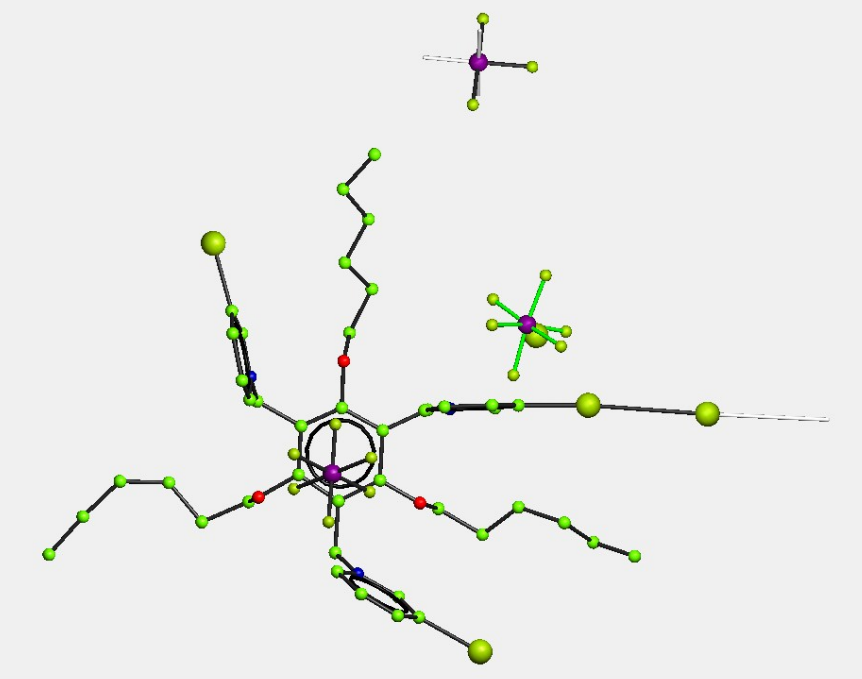

Figure S36: Partial refinement of the mixed PF_6^-/I^- salt of **4^{3+}**. Due to the very low quality of the data, it was not possible to achieve a stable refinement of this structure.

Structures of $3{\cdot}Br_3$ and $4{\cdot}Br_3$

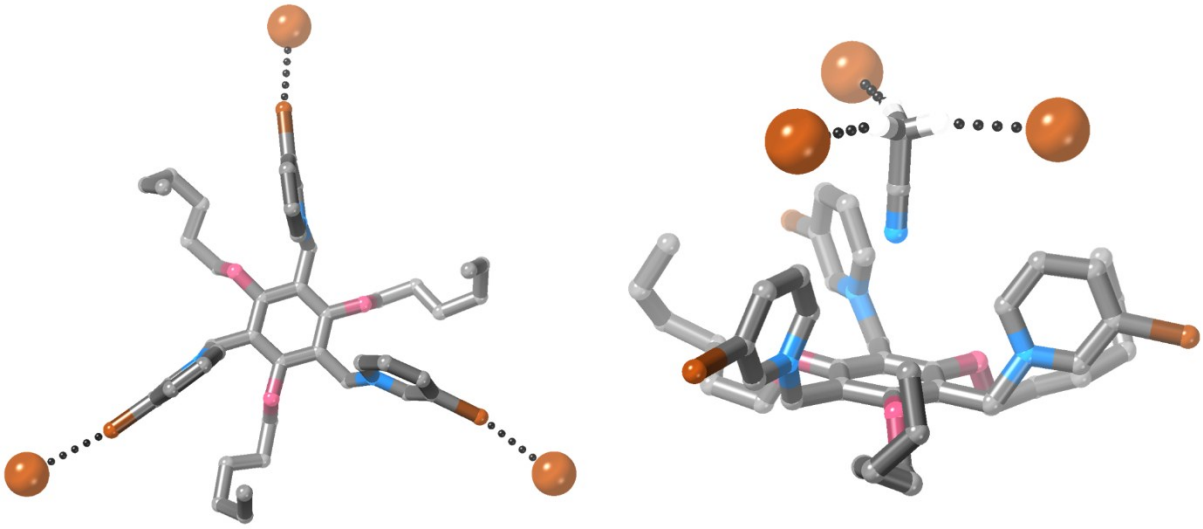

Figure S37: Two views of the crystal structure of **$3{\cdot}Br_3$** (most hydrogen atoms are omitted for clarity, as is the acetonitrile solvent molecule in the left view of the structure).

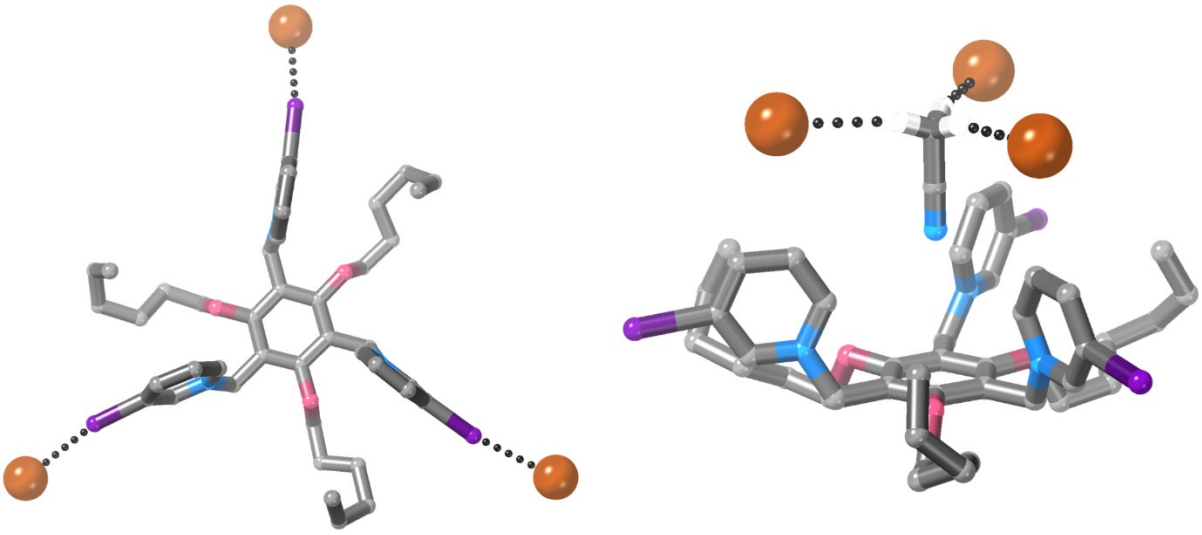

Figure S38: Two views of the crystal structure of **$4{\cdot}Br_3$** (most hydrogen atoms are omitted for clarity, as is the acetonitrile solvent molecule in the left view of the structure).

Table S1: Summary of crystallographic data

Compound	**3·$(PF_6)_3$**	**3·Cl_3**	**3·Br_3**	**3·I_3**
Radiation type	Cu (λ = 1.54184 Å)	Synchrotron (λ=0.71073 Å)	Cu (λ= 1.54184 Å)	Synchrotron (λ = 0.71073 Å)
Formula	C_{42} H_{57} Br_3 F_{18} N_3 O_3 P_3	C_{42} H_{61} Br_3 Cl_3 N_3 O_5	C_{44} H_{60} Br_6 N_4 O_3	$C_{42}H_{57}N_3O_3Br_3I_3$
Formula weight	1326.54	1034.03	1172.36	1272.33
a (Å)	8.50630(10)	14.104(5)	16.57730(10)	14.822(3)
b (Å)	25.6914(4)	25.266(9)	16.57730(10)	20.352(4)
*c (*Å)	24.6665(3)	14.735(4)	10.49130(10)	17.306(4)
Alpha (°)	90	90	90	90
Beta (°)	96.623(10)	115.280(19)	90	112.82(3)
Gamma (°)	90	90	120	90
Unit cell volume (Å^3)	5354.61(12)	4748(4)	2496.82(4)	4812(2)
Crystal System	Monoclinic	Monoclinic	Trigonal	Monoclinic
Space group	$P2_1/n$	$P2_1/n$	P-3	$P2_1/n$
Z	4	4	2	4
Reflections (all)	36746	25882	31656	34125
Reflections (unique)	10758	4954	3363	9760
R_{int}	0.0418	0.332	0.0476	0.0441
$R_1[I>2\sigma(I)]$	0.0971	0.2214	0.0406	0.0513
$wR_2(F^2)$	0.2784	0.2648	0.1390	0.1451
CCDC Number	1984628	1984629	1984630	1984631

Compound	**4·Cl·$(PF_6)_2$**	**4·$(PF_6)_{1.5}Br_{1.5}$**	**4·Br_3**	**4·I_3**
Radiation Type	Cu (λ = 1.54184 Å)	Synchrotron (λ=0.71073 Å)	Synchrotron (λ=0.71073 Å)	Cu (λ= 1.54184 Å)
Formula	$C_{43}H_{61}O_4N_3P_2F_{12}$	C_{42} H_{57} $Br_{1.5}$ F_9 I_3 N_3 $O_3P_{1.5}$	C_{44} H_{60} N_4 O_3 I_3Br_3	$C_{44}H_{60}N_4O_3I_6$
Formula weight	1390.03	1369.95	1313.42	1454.36
a (Å)	8.54400(10)	24.671(5)	16.639(2)	16.8999(10)
b (Å)	23.4300(2)	8.8760(18)	16.639(2)	16.8999(10)
*c (*Å)	27.3585(3)	23.946(5)	10.570(2)	10.9253(10)
Alpha (°)	90	90	90	90
Beta (°)	97.0540(10)	101.26(3)	90	90
Gamma (°)	90	90	120	120
Unit cell volume (Å^3)	5435.33(10)	5142.8(19)	2534.4(7)	2702.29(2)
Crystal System	Monoclinic	Monoclinic	Trigonal	Trigonal
Space Group	$P2_1/c$	P2/c	P-3	P-3
Z	4	4	2	2
Reflections (all)	41629	65940	33692	34563
Reflections (unique)	10691	11004	3893	3641
R_{int}	0.0518	0.1756	0.0654	0.0897
$R_1[I>\sigma(I)]$	0.0598	0.0812	0.0427	0.0565
$wR_2(F^2)$	0.1649	0.2833	0.1070	0.1516
CCDC number	1984632	1984633	1984634	1984635

References

1. G. R. Fulmer, A. J. M. Miller, N. H. Sherden, H. E. Gottlieb, A. Nudelman, B. M. Stoltz, J. E. Bercaw and K. I. Goldberg, *Organometallics*, 2010, **29**, 2176-2179.
2. www.supramolecular.org.
3. J. t. Cosier and A. Glazer, *J. Appl. Crystallogr.*, 1986, **19**, 105-107.
4. *CrysAlis Pro, Agilent Technologies.*
5. N. P. Cowieson, D. Aragao, M. Clift, D. J. Ericsson, C. Gee, S. J. Harrop, N. Mudie, S. Panjikar, J. R. Price and A. Riboldi-Tunnicliffe, *J. Synchrotron Radiat.*, 2015, **22**, 187-190.
6. T. M. McPhillips, S. E. McPhillips, H.-J. Chiu, A. E. Cohen, A. M. Deacon, P. J. Ellis, E. Garman, A. Gonzalez, N. K. Sauter and R. P. Phizackerley, *J. Synchrotron Radiat.*, 2002, **9**, 401-406.
7. W. Kabsch, *J. Appl. Crystallogr.*, 1993, **26**, 795-800.
8. G. M. Sheldrick, *Acta Crystallogr. A.*, 2015, **71**, 3-8.
9. G. M. Sheldrick, *Acta Crystallogr. C.*, 2015, **71**, 3-8.
10. O. V. Dolomanov, L. J. Bourhis, R. J. Gildea, J. A. Howard and H. Puschmann, *J. Appl. Crystallogr.*, 2009, **42**, 339-341.
11. L. J. Bourhis, O. V. Dolomanov, R. J. Gildea, J. A. Howard and H. Puschmann, *Acta Crystallogr. A.*, 2015, **71**, 59-75.
12. L. Palatinus and G. Chapuis, *J. Appl. Crystallogr.*, 2007, **40**, 786-790.
13. R. I. Cooper, A. L. Thompson and D. J. Watkin, *J. Appl. Crystallogr.*, 2010, **43**, 1100-1107.
14. P. W. Betteridge, J. R. Carruthers, K. Prout and D. J. Watkin, *J. Appl. Crystallogr.*, 2003, **36**, 1487.